Thesis Summary

Manganese Recycling from Spent Batteries Trough Electroactive Materials Synthesis

by

Romeo Robert Rácz
Dipl. Chem. Eng.
Faculty of Chemistry and Chemical Engineering, Babeș - Bolyai University, 2010

Submitted to the Department of Chemical Engineering
In Partial Fulfilment of the Requirements for the Degree of
DOCTOR OF PHYLOSOPHY IN CHEMICAL ENGINEERING

at the

BABEȘ - BOLYAI UNIVERSITY

November 2013

Signature of Author ________________________________
Department of Chemical Engineering
November 2013

Signature of Supervisor ______________________________
Petru ILEA
Professor of Chemical Engineering
Thesis Supervisor

SUMMARY

PART I

PART II

1. INTRODUCTION

Ever increasing production of consumer portable electronics established a new waste category composed of spent mobile energy sources. Stored improperly spent batteries represent an important environmental issue because of their heavy metal content. On the other hand waste electrochemical power sources represent a material group, which can be completely recycled thus avoiding pollution and generating added value products.

Literature review reveals the fact that manganese oxides are the most popular electrode material group used in primary and secondary cells. Manganese capability of having stable compounds with manganese oxidation states ranging from 2+ to 7+ largely explains the interest in energy for this material. Having multiple stable crystal structures allowed the development of intercalation materials for secondary batteries where a cathion is transported between the electrodes without ideally affecting the host structure.

Giving to the wide application of this material in electrochemical power cells the resulted spent, deteriorated or expired cells represent a growing waste sector. According to the literature, research has resulted two main approaches such as pyrometallurgical and hydrometallurgical treatment routes.

Pyrometallurgical treatment routes are based on bulk incineration of the spent battery amounts resulting solid metallic compounds and gases. Obtained solid phases are mainly composed of ferromanganese, metallic zinc while carbon-based materials are used to fuel the combustion process. Formed toxic gas phases are treated within the process. High-energy demands and resulted toxic gas volumes are considered the main disadvantages of pyrometallurgical processing. One notes the apparent advantage the important mass reduction trough treatment.

Hydrometallurgical spent battery processing consists of sorting spent batteries by type followed by mechanical, chemical and electrochemical treatment of the feedstock elements. In a typical hydrometallurgical processing flow chemical treatments are mainly composed of neutral, acidic and reductive leaching step. Resulted leaching liquors are either treated with selective chemicals or electrochemical processing for component separation. Main disadvantages are considered the handling of generated large liquid volumes and the existence of multiple stages of treatment. Low energy consumption, selective treatment, control over product purity and composition, flexibility towards treated material type and minimal environmental footprint are considered the main advantages of hydrometallurgical spent battery treatment routes.

The present doctoral thesis targets manganese recovery from spent batteries trough chemical and electrochemical processing resulting either valuable materials reusable in the recycling process or employable in the production of new Leclanché or Li-ion batteries. In order to meet the objectives fundamental and applicative research has been undertaken.

Research planning has considered the following objectives:

1. By recycling spent Zn – C batteries technically and commercially feasible materials must be obtained
2. Recovered materials must present electrochemical activity in the applicative spectrum
3. Development of a flexible processing route in order to adapt to feedstock and material requests variation

6. Titanium electrode in MnO_2 electrosynthesis

Literature reports a series of tested materials such as graphite (Ding, 2010), carbon nanotubes (Wang *et al.*, 2009), lead and it's alloys with Sn, Sb, Ag (Ilea *et al.*, 1997) and lately titanium as anodic substrate because electrocrystallized EMD is of higher purity than one obtained on other substrates (Ilea, 2005).

In electrochemical processes, when used as anodic material, the titanium's passivation is unwanted because of the low electric conductivity resulting in high-energy consumption. Nevertheless, in order to control this phenomenon several surface modification and passivation control techniques have been reported; literature lists as follows: surface coating with (3–5 μm) platinum film (Kholmogorov *et al.*, 2010), heated platinum plated Ti anode (Kononov *et al.*, 2007), RuO_2 and IrO_2 coatings (Wei *et al.*, 2010), anodic substrate activation through thermal-diffusion coating (Skopov *et al.*, 2010) β-PbO_2 coating and mixture of melted metallic titanium with graphite (Ilea, 2005). By surface modification with the previously listed techniques, a film can be developed which improves MnO_2 electrosynthesis on titanium.

In the present study based on previous observations (Rácz *et al.*, 2011a, 2011b), a study has been undertaken in order to investigate the electrochemical behaviour of polarized metallic titanium in solutions similar in composition with one resulted from spent battery lixiviation, with application in MnO_2 electrosynthesis from the above solutions.

Surface modification was required in order to use metallic titanium as a substrate for MnO_2 electrosynthesis. Several activation measurements have been performed in 1M H_2SO_4 and different concentrations of Mn^{2+}. An increasing number of MnO_2 germination centres on titanium have been noted with increasing manganese(II) ion concentration and have been considered for the fatherly-applied surface activation protocol. The as developed crystalline structures are electrically conductive bridges at the electrode-electrolyte interface and are considered the nucleation centres of the latter developing oxide layer.

6.1 Electrochemical corrosion measurements

Metallic titanium open circuit potential's (OCP) evolution was observed and registered, after immersion in 1M H_2SO_4 solutions in absence and presence of several Mn^{2+} concentrations.

A shift of the OCP values towards more positive potentials is observed in cases when different concentration of Mn^{2+} are present in the solution, as compared to metallic titanium in sulphuric acid solutions without additives, suggesting an interaction of Mn^{2+} with the anodic reaction of the corrosion process.

Polarization measurements were carried out in order to characterize the corrosion behaviour of the metallic titanium surface by applying the Stern - Geary theory (Stern and Geary, 1957) and by using Tafel interpretation.

Following the intricate active – passive behaviour of pure titanium in highly acidic sulphate solutions, the obtained polarization curves do not exhibit typical Tafel behaviour, accurate evaluation of the corrosion not being possible. However, the values of ε_{corr} and the corrosion current density, i_{corr}, were evaluated near zero-overall current on the potential range of +250 and -250 mV vs. OCP with a sweeping rate of 0.166 mVs^{-1}. Evaluated parameters for the corrosion process are presented in Table 6.1.

Table 6.1. Parameters of the metallic titanium corrosion process

Solution	ε_{corr} (mV vs. REF)	i_{corr} ($\mu A/cm^2$)	$-b_c^*$ (mV^{-1})	b_a^* (mV^{-1})
1M H_2SO_4	-0.2	19	89	218
1M H_2SO_4+ 3g/L Mn^{2+}	-0.1	17	155	161
1M H_2SO_4+ 6g/L Mn^{2+}	0	15	98	139
1M H_2SO_4+ 9g/L Mn^{2+}	0.05	12	103	110
1M H_2SO_4+ 12g/L Mn^{2+}	0.04	10	86	118

*b_a and b_c are the Tafel anodic and cathodic activation coefficients

From the data presented in Tab 6.1, positivation of the titanium's corrosion potential (ε_{corr}) can be noted, which corresponds to active corrosion inhibition of the metallic surface.

6.4 Voltammetry measurements (Rácz *et al.,* 2011a, 2011b)

Linear voltammetry curves (LVC), presented in Fig. 6.2, reveal four voltage regions: (i) active corrosion, (ii) active-passive transition, (iii) passivity and (iv) the voltage beyond which the dielectric breakdown of the passive film occurs. These observations are in good agreement with the cited literature (Hosseini și Sigh, 1993; Utomo și Donne, 2006). Each region from the polarization curve corresponds to different reactions, which occur with potential positivation.

Concurrent reactions (Utomo și Donne, 2006) increase the number of geometrical faults in the formed TiO_2 layer and help the current passage.

The recorded polarization curves, with the addition of Mn^{2+} are presented in the inset of Fig. 6.2, showing a clear dependence of the peak current with increasing Mn^{2+} concentration.

It is also notable that the presence of Mn^{2+} ions modifies the polarization curve's profile in region (iv), resulting in the breakdown of the insulating layer by the oxidation of manganese ions at ε_{ox}=~ 1.4 V/REF.

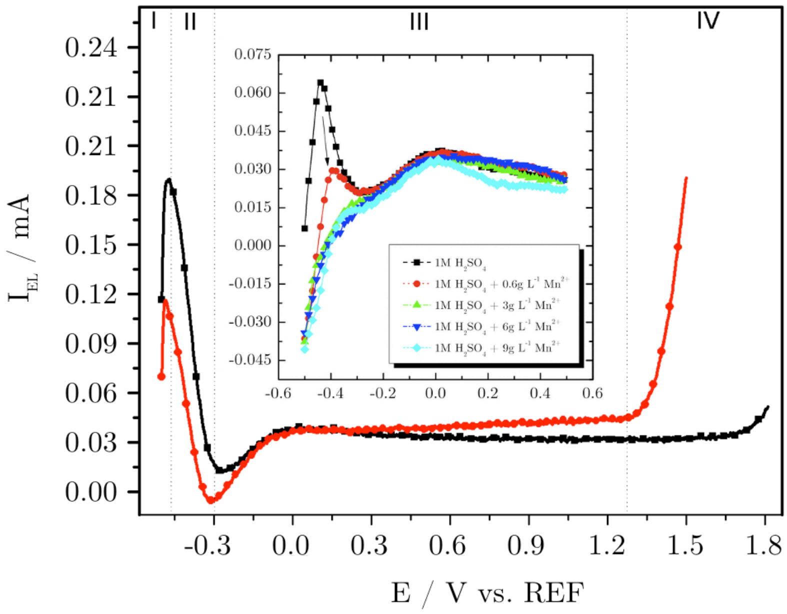

Figure 6.2. Metallic titanium polarization curves in the absence (n) and presence of Mn^{2+} ions ( ). Inset: Titanium oxidation peak current evolution with the addition of different Mn^{2+} concentration

EMD crystal structures have been observed on the titanium surface by scanning electron microscope. Occurrence of these manganese oxides on the anodic surface leads to structural faults in the TiO_2 film, which leads to the breakdown of the so formed titanium oxide thin film and allows the oxidative electrosynthesis to occur.

6.5 Electrode modification

Surface modification was required in order to use metallic titanium as a substrate for MnO_2 electrosynthesis. Several activation measurements have been performed in 1M H_2SO_4 and different concentrations of Mn^{2+}. By visual examination, an increasing number of MnO_2 germination centres on titanium have been noted with increasing manganese(II) ion concentration and have been considered for the fatherly applied surface activation protocol.

The electrode surface modification was achieved in three steps and represents the surface activation protocol.

Metallic titanium has been immersed in a solution containing 6g/L Mn^{2+}. In the first step (S1) the potential was modified with 2 mVs^{-1} in the range from 0 to 1.5V/ REF. During the second step (S2) the potential has been set to zero and kept at this value for 10 seconds. During (S3) the potential has been modified in the range from 1.5 to 1.7V/REF with $2mVs^{-1}$.

The switch from S1 to S2 was made by current interruption for 10 seconds and was considered responsible for the mentioned phenomena on the observed surface as graphically describe in Fig. 6.4.

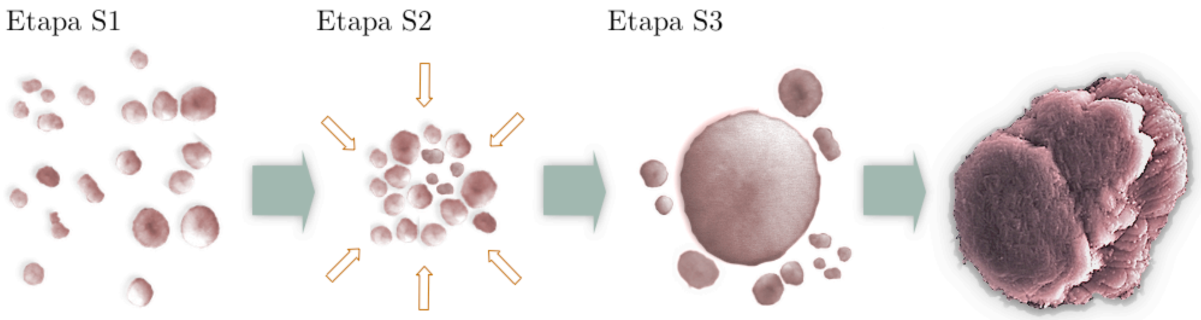

Fig. 6.4 Stages of the crystalline structure's transformation on Ti surface

The potential value was varied below MnO_4^- formation and oxygen evolution reaction at the electrochemical conditions.

6.6 MnO_2 electrolysis tests

The activated titanium electrode was inserted in a divided cell setup, composed by a modified titanium electrode (MTE), platinum counter electrode (PCE), $Ag||AgCl/KCl_{sat}$ reference electrode and a porous ceramic material for MTE separation from PCE.

During 4 hour of continuous electrolysis the MTE did not exhibit passivation or critical behaviour (Fig. 6.5b).

Under continuous stirring and constant temperature (22°C) a film of MnO_2 was deposited on the modified titanium surface from an acidic sulphate solution containing 6 g/L Mn^{2+}.

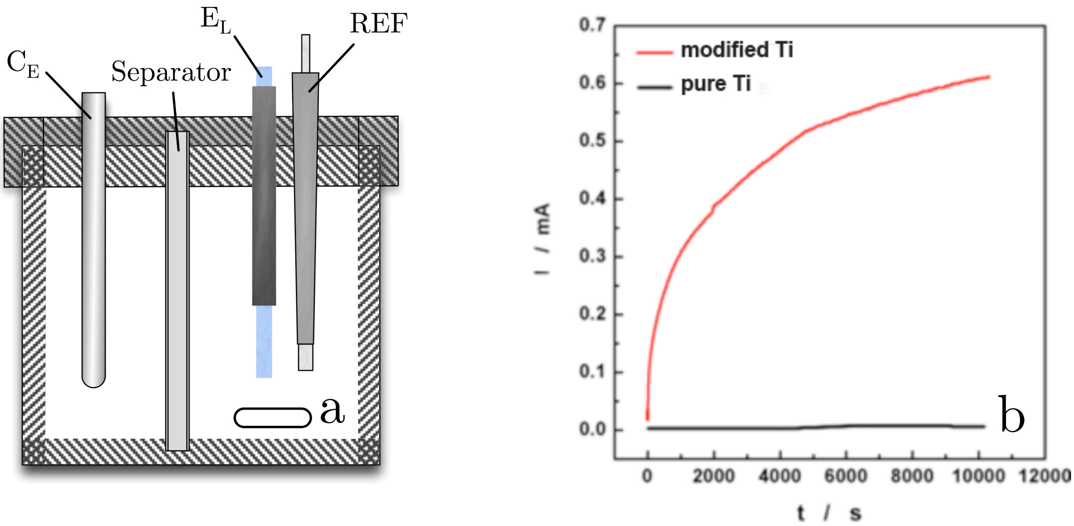

Fig. 6.5 a) Divided electrochemical reactor b) current evolution under potentiostatic control in 1M H_2SO_4 Mn^{2+} 6g L^{-1} stirred electrolyte.

7. SIMULTANEOUS Zn AND Mn_3O_4 ELECTROWINNING

The aim of this study is to establish operating parameters for the electrochemical recovery of zinc and manganese oxides from spent battery leaching liquors in form of valuable products.

The electrochemical cell used in this study has been entirely manufactured from Plexiglass^{TM} (poly-methyl methacrylate) as shown in Fig. 7.1. The system featured an electrolytic membrane reactor and a computer controlled DXC 236 potentiostat/galvanostat. As cathode, a thin aluminium sheet has been employed. Aluminium is used owing to the poor adhesion of the deposited zinc, which can later be easily removed.

As anode, a sheet of Pb-Ag has been used. A layer of lacquer has been applied on the backside of the electrodes for insulation purposes resulting an effective surface of S=7,5 cm^2 in both cases. A computer aided power supply applied current to the reactor, and registered electrode and cell voltages in an online fashion. The anion exchange membrane employed to separate the anode and cathode compartments in this study consists of a polystyrene gel structure cross linked with divinylbenzene, quaternary ammonium functional groups supplied by Membranes International, Inc.

7.3 Spent battery material composition and leaching

According to XRD measurements of the spent battery material a large number of clearly identifiable materials have been noted, such as Mn_3O_4, Mn_2O_3, iron containing compound, chlorine and manganese hydroxides. Fig. 7.2 Registered XRD spectrum for the spent Zn - C battery material

During discharge the following overall electroactive reaction occurs in a Zn – C dry battery (Shin et *al.,* 2009):

$$Zn + 2MnO_2 \rightarrow Mn_2O_3 + ZnO \qquad (7.1)$$

Since ZnO represents the main Zn discharge product present in the black powder, an acid solution (1M - H_2SO_4) readily dissolves it (Anton et *al.,* 2011). Other manganese oxides (MnO) formed during discharge, are successfully leached as well, according to the following reaction (de Michelis et *al.,* 2007):

$$ZnO + H_2SO_4 \rightarrow ZnSO_4 + H_2O \qquad (7.2)$$

Leaching of the other manganese discharge products such as Mn_2O_3 and Mn_3O_4 is partial (de Michelis et *al.,* 2007) due to the formation of insoluble MnO_2.

$$Mn_2O_3 + H_2SO_4 \rightarrow MnO_2 + MnSO_4 + H_2O \qquad (7.4)$$

7.4 Electrochemical study of the Pb-Ag substrate (Rácz and Ilea, 2013)

The Pb-Ag anode was subjected to polarization by sweeping potentials from the open circuit potential (OCP) value to 2V. A redox couple has been identified (Fig. 7.3left) in the range of $-0.5V<E<-0.25V$ corresponding to the dissolution of lead to form $PbSO_4$ and reverse, as shown in reaction (7). After the oxidation peak identified at -0.412V, passivation of the electrode occurs due to the formation of non-conductive $PbSO_4$ (Pavlov and Iordanov, 1970):

$$Pb(s) + H_2SO_4 \rightarrow PbSO_4(s) + 2H^+ + 2e^- \qquad E^\circ = -0.358\ V \qquad (1.28)$$

Fig. 3b shows registered currents on the potential domain from 1V to 1.8V vs. the reference electrode (RE) in presence and absence of Mn^{2+} and Zn^{2+} species. The value of 1.8 V has been chosen as cut-off voltage, given the fact that, processes occurring at more positive potentials are not distinguishable from the cyclic voltammetry profiles.

In the absence of Mn^{2+}, after passive behaviour, at more positive potentials, activation of the substrate is noted by the appearance of a peak (I) at 1.72 V vs. RE. At the reverse scan, a reduction peak is noted at 1.33 V vs. RE. Meanwhile, in presence of 6gL^{-1} Mn^{2+} (zone II) undergoes a similar oxidation process (to one shown in Fig. 7.3right), reaching higher anodic current values. At more positive potentials, after the presented peaks, OER is occurring (not shown). During the reverse scan, considerably lower cathodic currents are registered in the broader potential range of 1.2 V< E <1.4 V with a maximum current value at 1.34 V vs. RE. In the presence of both 6 gL^{-1} Mn^{2+} and 65 gL^{-1} Zn^{+2} (zone III) no major difference is noted in comparison with the previously completed case (zone II).

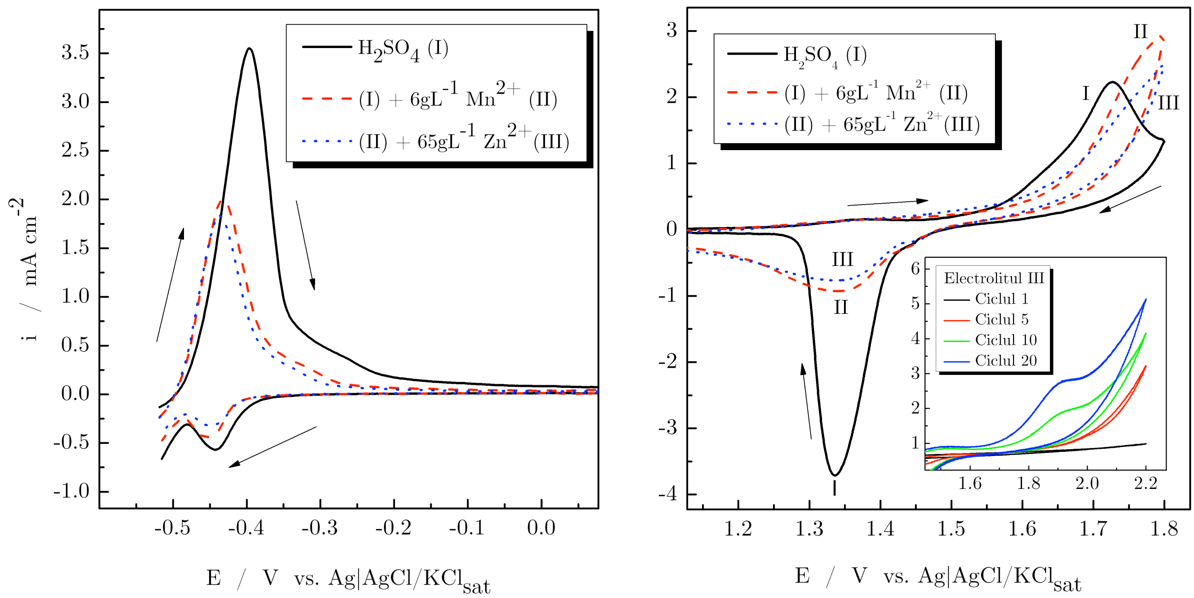

Fig. 7.3 Registered cyclic voltammograms for the Pb-Ag substrate in electrolytes (i) – (iii).

Effects of iron concentration [Fe^{2+}] > 0.01M reported in the literature (Pilla et *al.*, 2009), do not represent an issue in the present electrochemical setup due to the low concentration of ≈190mg L^{-1}. Moreover, the electrochemical activity is limited to oxidation. The obtained manganese oxides during electrolysis tests do not contain iron as confirmed by XRD measurements.

7.5 Simultaneous electrowinning of Zn and Mn_3O_4

During simultaneous electrowinning of SBLL and remnant zinc casings leaching liquor, extraction of manganese oxide and zinc occurs in the setup presented in Fig. 7.4. As generally known, the higher the Zn^{2+} concentration the higher the current efficiency of zinc electrowinning, following Wark's rule (Wark, 1963).

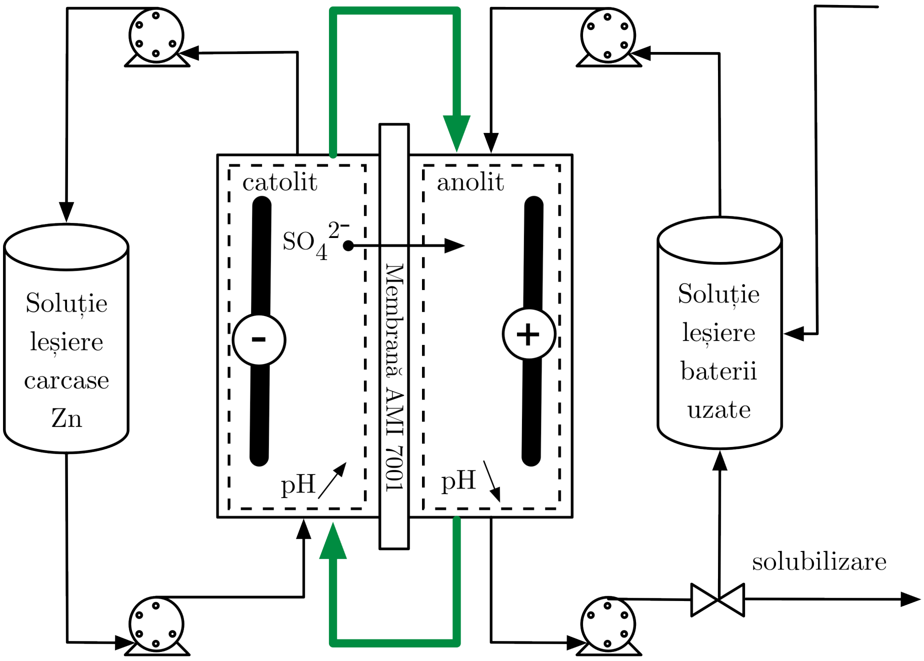

Fig. 7.4 Scheme of the experimental setup employed in this study

A lower pH will positively stimulate the deposition process in presence of the manganese ions, making the recirculation of the fluxes possible without additives, between electrowinning processes.

During polarization, a non-conductive $PbSO_4$ layer formed on the anode surface resulting in current and potential increase of the unreacted surface.

The generated $PbSO_4$ and the unconverted lead transforms to PbO_2, followed by the oxidation of Mn^{2+} at higher anodic potentials. When a steady layer of PbO_2/MnO_2 has formed the reaction reaches an equilibrium resulting stabilisation of the potential at the macroscopic level (Lai et *al.* 2010). These events makes anodic potential increase rapidly, initially, and then gradually becoming stable.

Under galvanostatic control, with different current intensities the potential's value during electrolysis stabilises at the anode (E_{anode}) between 1.7V and 1.85V vs. RE and between -1.0V and -1.2V vs. RE at the cathode ($E_{cathode}$).

Manganese oxidation on the anodic surface occurs with highest yield in the experimental set up of this study. At a current density of 50 mA/cm^2 the anodic current efficiency is 85% and decreases with increasing current intensities as shown in Tab. 7.3.

Tab. 7.3. Electrolysis operating parameters and results

Current density	Anode			Cathode			Cell voltage
	E_{anode}	Current efficiency	pH	$E_{cathode}$	Current efficiency	pH	
[mA/cm²]	*[V]*	*[%]*		*[V]*	*[%]*		*[V]*
25	1.69	59	0.2	-1.06	84	2.7	4.7
50	1.73	85	0.5	-1.1	91	2.6	4.4
100	1.78	72	0.3	-1.14	89	2.6	5.1
200	1.81	42	0.3	-1.15	70	2.6	5.8

Spent electrolyte streams resulted from the first run consists, in the case of the anolyte a concentration of 65g/L Zn^{2+} and traces of Mn^{2+}. This has been considered suitable for high yield zinc deposition (Zhang and Hua, 2009) without further purification and has been directed to the cathodic compartment. The catholyte after exhaustion is low in concentration of both Zn^{2+} and Mn^{2+} and has been regenerated for further use as a lixiviant in the SBM solubilisation step by assuring required solid-liquid ratio and acid concentration.

7.6 Deposits structural analysis by XRD

Fig. 7.6 shows the XRD pattern of the manganese oxide and zinc obtained by electrolysis at 50mA cm^{-2}.

Manganese oxide diffraction peaks in the pattern, can be indexed to tetragonal hausmannite Mn_3O_4 (space group *I*41/*amd*) with lattice constants of a = 5.76 Å, c = 9.47 Å corresponding to that of JCPDS 24-0734. The diffraction peaks can be assigned to (101), (112), (200), (013), (211), (004), (105), (220) and (015) planes of the hausmannite Mn_3O_4 with tetragonal structure. Diffraction peaks of the cathodic deposit can be indexed to the metallic Zn (space group *P*63/mmc) with lattice constants a = 2.66 Å, c = 4.94 Å corresponding to that of JCPDS 65-3358. Peaks can be assigned clearly to (002), (100), (101) and (012) planes of the hexagonal pure Zn structure. The strong and sharp reflection peaks suggest that the as obtained deposits are well crystallized. Peak broadening indicates small crystallite sizes and has been approximated with Scherrer's equation. In the equation β is the full width at half maximum (FWHM) in radians, the shape factor K has been assumed to be 0.9, λ is the employed X-ray wavelength, ϑ the corresponding Bragg-diffraction angle. Estimated coherence lengths (L_c) have been found to be in the nano-metric range with medium values of $L_c \approx$ 29nm for zinc and $L_c \approx$ 13nm for Mn_3O_4.

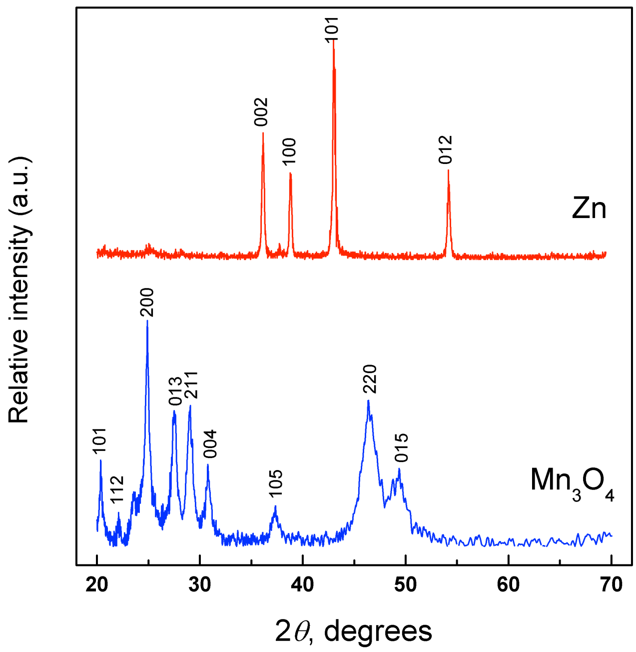

Fig. 7.6 X-ray diffraction pattern of the electro-synthetized Zn and Mn_3O_4

7.7 Deposits morphological analysis by SEM

Figure 7.7a shows SEM micrograph of the cathodic deposits obtained at 50mA cm^{-2}, composed by nanometric plate-like intergrowth structure with particles of 10-15nm thickness and several tents of nanometre wide. Size and shape distribution is evenly distributed with dendritic agglomerations at higher electrowinning current densities at the electrode edges (not shown). Anodic deposits consist of unevenly distributed porous, flake-like agglomerations (Fig. 7.7b).

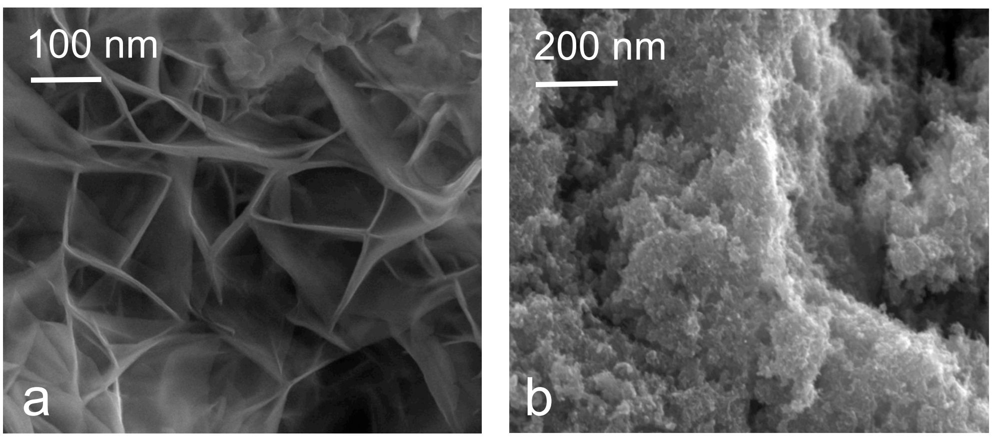

Fig 7.7. (a) SEM micrographs of cathodic deposits obtained at 50mA cm^{-2}, (b) anodic deposits obtained at 50mA cm^{-2} from spent battery leach liqour

EDX scans of the cathodic deposit (Fig.7.8a) shows mainly contribution from zinc, followed by sulphur and oxygen which originate from SO_4^{2-} in the solution and could not be removed by washing prior to the measurement. Elemental analysis of the anodic product (Fig.7.8b) reveals contribution of elements (Mn, O, S) in deposit structure and interference from elements of the anodic substrate (Pb, Ag).

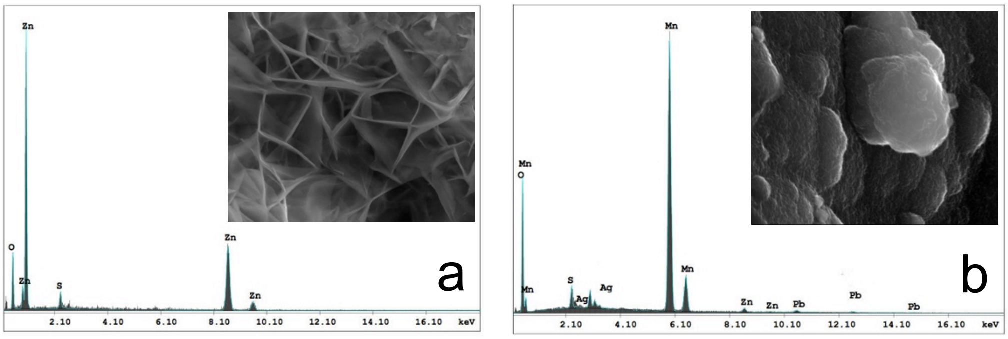

Fig. 6 EDX spectra of a) cathodic deposit and b) anodic deposit

Based on literature information and preliminary experimental results, a hydrometallurgical process flowsheet has been proposed for complete recycling of spent, deteriorated or expired Zn-C batteries. In the studied electrochemical setup high purity nano-metric zinc and Mn_3O_4 has been simultaneously electrodeposited from spent battery leach liquors in an anionic membrane reactor. Electrowinning tests have shown best results in current efficiency terms at a current density of 5A dm^{-2} yielding 91% for zinc and 85% for manganese oxide electrowinning efficiency, consistent with typical plant practice. Obtained values are superior or equal with ones reported (Ault and Frazer, 1988; De Souza, 2004, Zhao and Liu, 2011). Information about structure, composition and morphology of the electrosynthetized deposits has been obtained by applying XRD, EDX, SEM and electrochemical measurements revealing phase pure Zn and Mn_3O_4.

8. MnO_2 MICROWAVE-ASSISTED CHEMICAL SYNTHESIS

In the present study synthesis and characterisation of different MnO_2 phases have been explored as intercalation materials in Li-ion type cells. Employed microwave-assisted hydrothermal synthesis route yields well crystallized and phase pure α-, β-, δ-, and mixed α-β- and α-γ- MnO_2 structures which can reversible accommodate Li^+ ions during constant discharge at different loads. Cycling rate capabilities have been found to exhibit constant behaviour at C/10 discharge rate for β-MnO_2 phase, resulting 150 mAg^{-1} for 50 cycles with the accommodation of up to 0.7 Li^+ per Mn. Obtained mixed oxide phases have been compared with the pure phases regarding capacity and cycling behaviour during lithium insertion. Obtained materials have been characterized for their structure and morphology by XRD, HRTEM and SEM, Li^+ intercalation and de-intercalation by electrochemical techniques such as cyclic voltammetry, galvanostatic cycling with potential limitation (GCPL) and electrochemical impedance spectroscopy (EIS).

Phase-pure MnO_2 polymorphs have been successfully synthetized from known precursors with a low reaction time and temperature with a microwave-assisted heating approach. In the present hydrothermal route the precursor set reaches reaction temperature in an intensified fashion (600 seconds), with homogenous temperature gradients in the reaction volume followed by fast cooling.

Several key process parameters such as temperature, synthesis time, precursor concentration and additives have been found to exert high impact on the formation of different MnO_2 crystal structures. During MW synthesis, pure, mixed and amorphous phases have been obtained, however here we present the modification of precursor set and the reaction temperature's influence. Reaction temperatures have been varied between 100°C and 200°C and also represent the chosen limits, since above and beyond these values no reaction occurs or the more thermodynamically stable β-MnO_2 phase predominantly forms. Pure and mixed phased MnO_2 polymorphs have been synthesized by employing the following chemical reactions in presence of microwaves:

$$3MnSO_4 + 2KMnO_4 + 2H_2O \rightarrow 5MnO_2 + K_2SO_4 + 2H_2SO_4 \quad (8.1)$$

$$MnSO_4 + (NH_4)_2S_2O_8 + 2H_2O \rightarrow MnO_2 + (NH_4)_2SO_4 + 2H_2SO_4 \quad (8.2)$$

$$Mn(NO_3)_2 + \tfrac{1}{2}O_2 + H_2O \rightarrow MnO + 2HNO_3 \quad (8.3)$$

$$3MnSO_4 + 2KMnO_4\,(\text{exces}) + 2H_2O \rightarrow MnO_2 + K_2SO_4 + H_2SO_4 \quad (8.5)$$

$$KMnO_4 + H_2O_2 \rightarrow K_{1.33}Mn_8O_{18} + H_2O \quad (8.6)$$

Solution pH values have not been altered and together with other parameters are summarized in Tab. 8.1. Further chemistries have been tested by adding stoichiometric amounts of $(NH_4)_2SO_4$ and Li_2SO_4 to the above reactions, but no notable effect has been recorded by means of product purity or electrochemical activity. For further investigations only the pure products and selected mixed phases have been used.

Synthetized products have been characterized by means of X-ray diffraction by a Shimadzu XRD – 6000 diffractometer with Cu-cathode with $K_{\alpha 1}$ and $K_{\alpha 2}$ lines (λ = 1.54178) in Bragg-Brentano geometry with a max power output of 3 kW. The measurements were taken in the range from 20° to 70° with a step size of 0.02 and integration time of 7s per step. Rietveld refinement and calculation of lattice parameters and structure, was done using FullProf Suite 2.0. Manganese oxides have been morphologically examined by SEM (Gemini, Zeiss) with acceleration voltages between 7kV and 10kV. Prior scanning samples have been coated with a 10nm layer gold by sputtering (Balzers Union). HRTEM analysis of the products has been done using (KRONOS, Zeiss). Specific surface measurements have been carried out by Brunauer-Emmett-Teller (BET) theory in an in-house built device.

8.4 MnO_2 structural analysis by XRD

Manganese dioxide polymorphs are formed by the different interlinking of the MnO_6 octahedra resulting 1D, 2D and 3D tunnel structures (. Discrimination of the different crystallographic structures can be achieved by the tunnel (size) diameter formed by the MnO_6 unit. The structure of α-MnO_2 is composed by (2x2) and (1x1) one-dimensional channels forming tunnel structures along *c*-axis framed by interlinking of MnO_6 chains. Usually these spaces are occupied by structure stabilizing cations (Na^+, NH_4^+, K^+, B^+) or H_2O molecules (Thackeray, 1997). β-MnO_2 is of rutile structure with tetragonal symmetry, oxygen ions forming hexagonal-closed-packed arrays. The interstitial spaces consist of 1D (1x1) channels formed parallel with the crystallographic c-axis. γ-MnO_2 consists of random intergrowth of ramsdellite (2x1) and pyrolusite (1x1) domains, described by de Wolff Thackeray, 1997) disorder and microtwinning, while δ-phase is a 2D layered structure (Fig.1d) with stabilizing cations (NH_4^+, K^+, Li^+) and H_2O molecules in the interspace region. Accommodation of Li^+ can be expected in MnO_2 polymorphs being limited only by the presence of structure stabilizing cations. Structural refinement yields parameters in accordance with the literature (Thackeray, 1997) and has been summarized in Table 1.

Tab. 8.2 Obtained crystal structure parameters from Rietveld refinement

Phase	Simetry	Space group	Structural parameters a (Å)	b (Å)	c (Å)	α (°)	β (°)	γ (°)	Vol. ($Å^3$)	Tunnel*	Dim** (nm)
α	Tetragonală	I4/m	9.801	9.801	2.850	90	90	90	273.6	(2x2)(1x1)	16
β	Tetragonală	$P4_2$/mnm	4.402	4.402	2.872	90	90	90	55.6	(1x1)	27
δ	Triclinică	C2/m	5.130	2.845	7.503	90	101	90	107.3	straturi	8

Observed peak broadening in the XRD spectra indicate small crystallite sizes and has been evaluated by applying Scherrer's equation. Results have been summarized for each phase in Tab. 8.2., where β is the full width at half maximum (FWHM) in radians, the shape factor K has been assumed to be 0.9, λ is the employed X-ray wavelength, θ the corresponding Bragg-diffraction angle. Estimated coherent lengths (L_c) have been found to be in the nano-metric range, in accordance with SEM and HRTEM measurements.

Obtained XRD patterns of the synthetized α-MnO_2 phase can be indexed to the space group JCPDS card No. 44-0141 with structural parameters summarized in Table 1. No other peaks have been identified in the pattern, indicating a high-purity product. Diffraction data collected for β- and γ- phases suggest formation of highly crystalline material indexed with JCPDS no. 24-0735 and JCPDS no.14-0644 respectively, with no peaks attributable to other phases. However, impurity phases have been detected during synthesis parameter tuning, mainly consisting of amorphous phases, $NH_4Mn_2(SO_4)_3$, K_2SO_4, NH_3NO_3, for which XRD data has not been shown. MW synthesis also resulted mixed polymorphs with different ratios. Powder diffraction patterns have been labelled accordingly.

8.4 MnO_2 structural analysis by SEM

Morphological analysis of the obtained MW synthetized MnO_2 polymorphs revealed mainly 2D needle-like rod structures for each pure phase. However the particle dispersion and stacking is different in size and arrangement. Obtained α-phase consists of 80-100nm rod-like structures resulted by the condensation of 10-15nm needle-like formations as shown in Figure 3a. δ-phase is composed by lamellar structures assembled in plate-like formations with average widths around 100nm as shown in Figure. 8.3d.

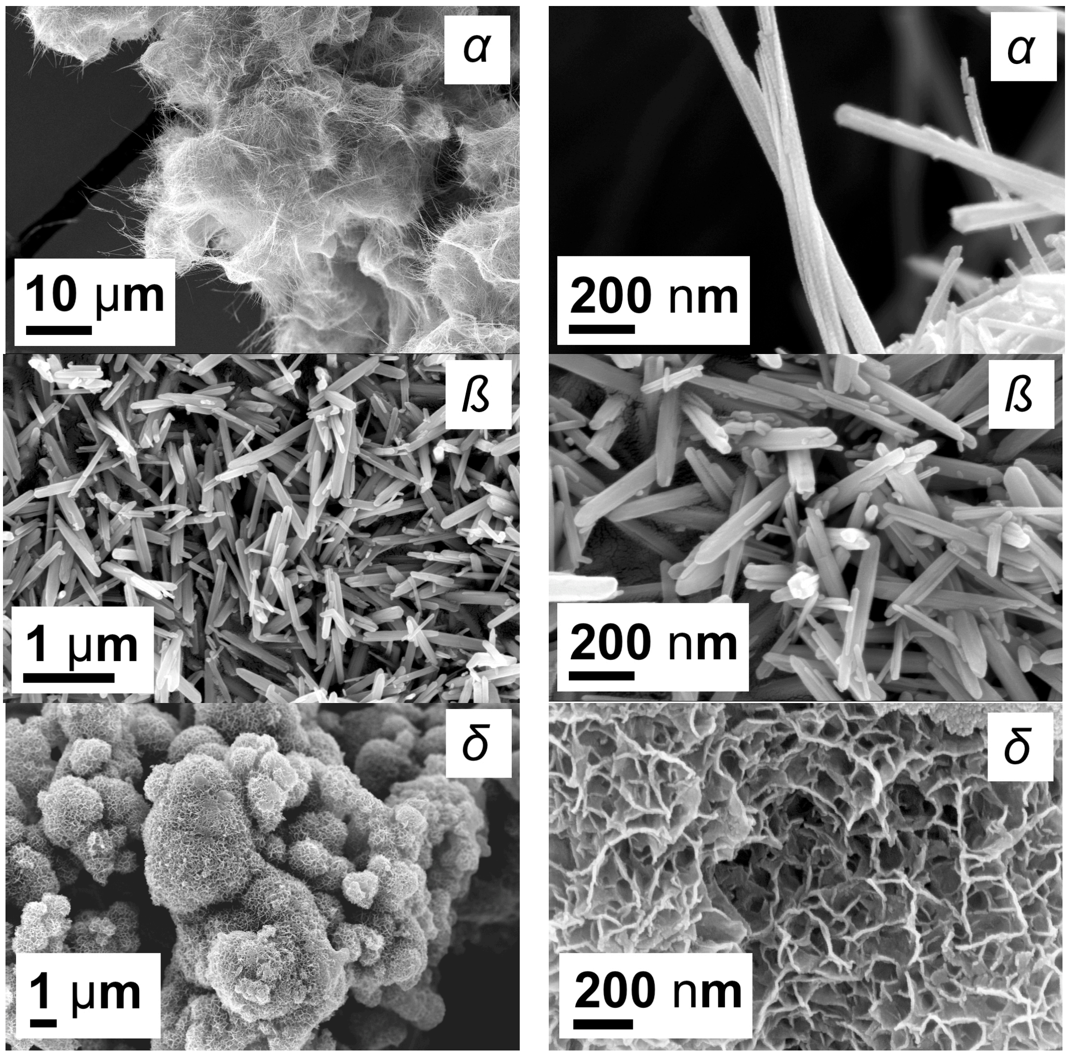

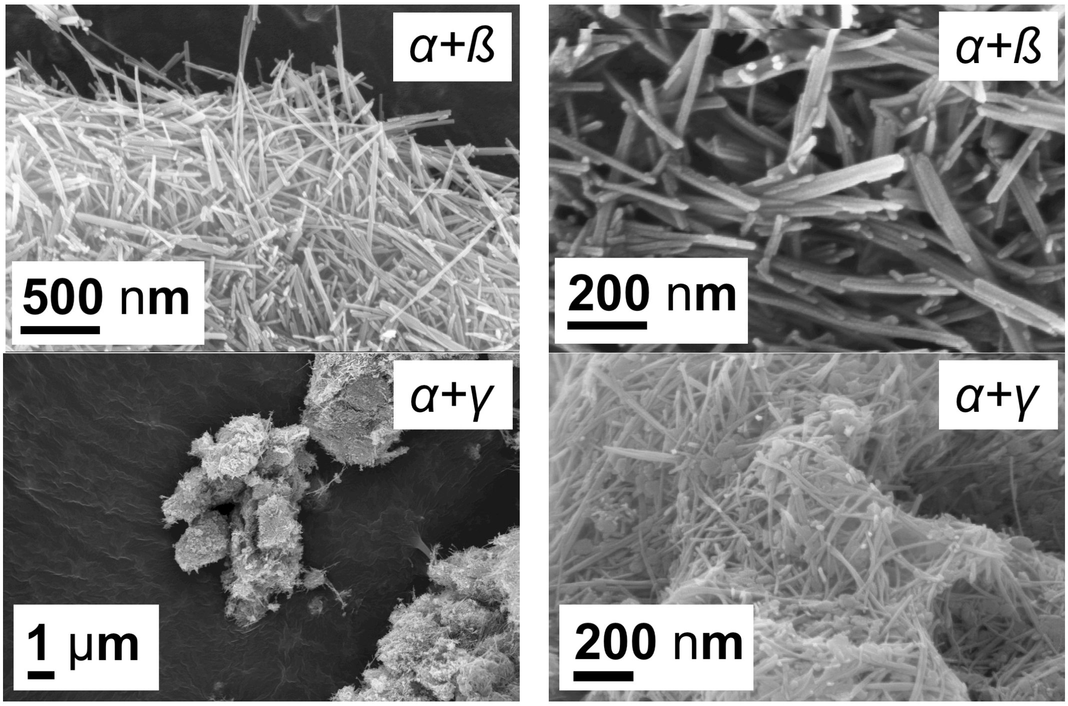

Fig. 8.3 SEM micrographs obtained for different synthetized material

8.6 MnO_2 electrochemical characterisation

Fig. 8.4a displays recorded voltammograms for α-MnO_2 where during the first cycle starting from the open circuit potential (OCP) a broad reduction peak is observed at 2.26V vs. Li|Li^+ resulted from the accommodation of Li^+ in the α-MnO_2 framework. At the reverse scan a peak is observed at 3.12V. Initially a double peak profile is obtained, but during cycling this merges into a single peak shape (Fig, 8.4a).

In the case of pure β-MnO_2 phase the first intercalation cycle occurs at 2.32V vs. Li|Li^+ jumping and stabilizing to around 3V (Fig.8.4b) in the next cycles. Peak formation upon cycling at above 4V can be attributed to the transformation of the β-MnO_2 into the framework of $[Mn_2]O_4$ of $Li_x[Mn_2]O_4$ spinel or defect rock-salt structures. Fig. 4d displays broad redox peak pairs for Li^+ intercalation in the microwave synthetized phase-pure δ-MnO_2 structure at 2.75V and de-intercalation at approximately 3V. Upon cycling the material exhibits stable behaviour with no additional peaks appearing after the unidentifiable peak-pair at 3.75V, which fades after the 1st cycle. Broadness of the redox peaks has been largely attributed to the nanostructured nature of the material. Mixed phase oxides present a less stable behaviour for α-,γ-MnO_2 (Fig.8.4e) where lithium insertion occurs between 2.25V$<E_{red}<$3V vs. Li|Li^+ showing stability in the last two cycles at approximately 2.9V with an slight increase in the peak current. The unstable nature of α-phase resulted from structural collapse from 2x2 to 1x2 irreversible form of the ramsdellite structure, which here has been synthetized as-is. The peak potential shifting in the as-synthetized material could be attributed to the collapse of the contained 2x2 tunnel structures and the occurred stabilization at phase equilibrium, which can withstand the expansion suffered during Li^+

accommodation. However, the overall reversibility of the electrochemical process can be noted. Fig. 4f shows the electrochemical response of the mixed α-, β-MnO_2 phase. Similar peak potentials with the pure β-phase can be observed, but with lower peak currents and no clear presence of the oxidation peak at 4.2 V observed in Fig. 8.4b, attributable to the transformation of the rutile structure to the spinel frame.

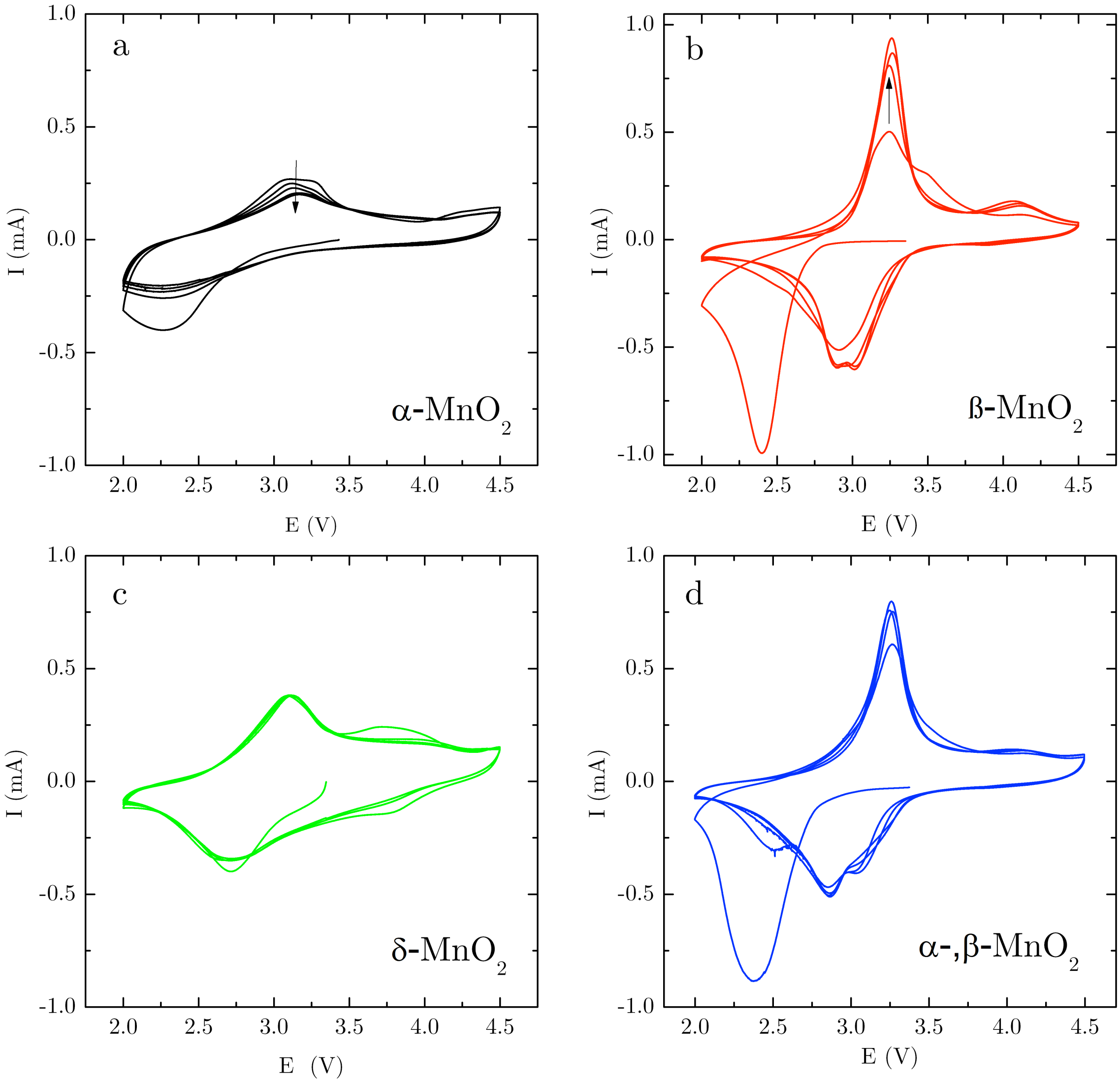

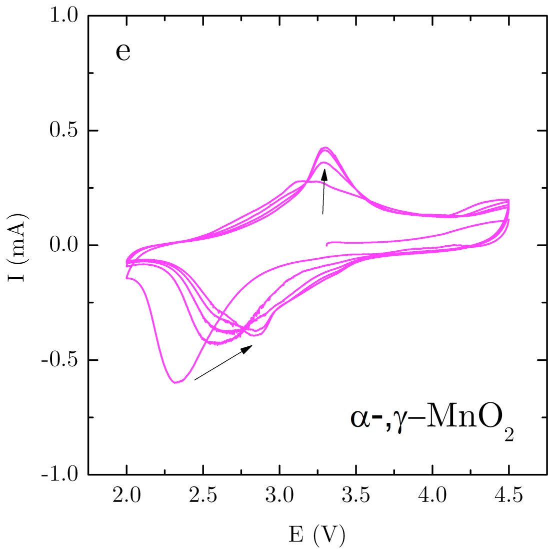

Fig. 8.4 Registered voltammograms for different MnO_2 polymorphs synthetized in a microwave assisted chemical reactor Sweep rate: 0.1mV s^{-1}, electrolyte: $LiPF_6$, temperature 25°C.

Fig. 8.5 presents measured capacities and capacity retention during GCPL tests at different loads. Materials exhibit a first-cycle maximum capacity of 281 mAh g^{-1} for β-MnO_2 at C/100. A value of 240 mAh g^{-1} has been obtained at C/20 in the case of β-MnO_2 accommodating a maximum of 0.7 Li^+ per Mn. However, the initial high discharge rate drops to 161 mAh g^{-1} displaying a stable trend during the following cycles. At above 100 charge-discharge cycles a constant 0.5 Li^+ per Mn is obtained providing 483Wh kg^{-1} at C/10 discharge rate. Fig. 8.6 illustrates the different discharge behaviours for synthetized MnO_2 polymorphs. During GCPL tests, ß-MnO_2 exhibits a plateau-like behaviour during discharge at around 3V. Alpha and gamma phases quickly decline with an increasing sloping voltage.

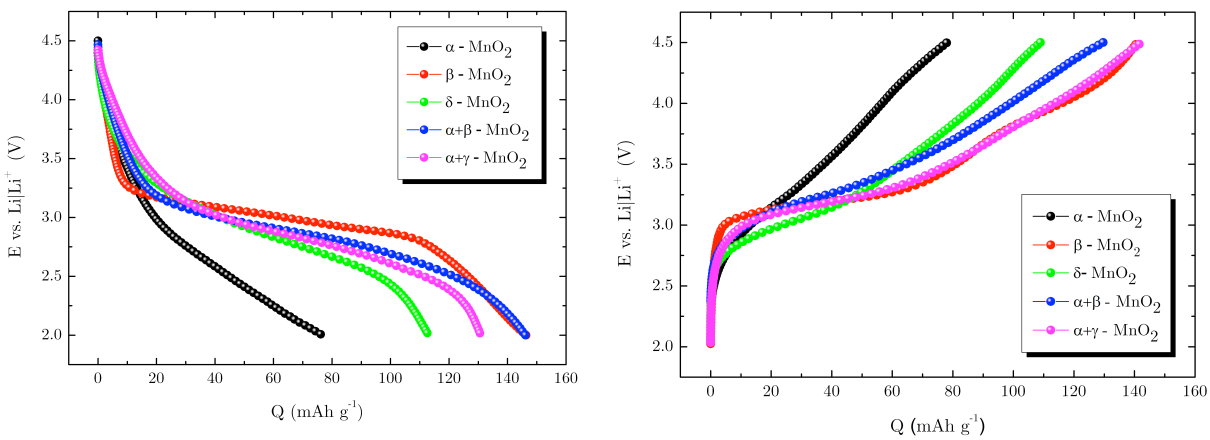

Fig. 8.5 Galvanostatic discharge-charge tests at C/10 Electrolyte: $LIPF_6$

Materials have been tested for their capacity retention during galvanostatic cycling with potential limitations as shown in Fig. 8.6.

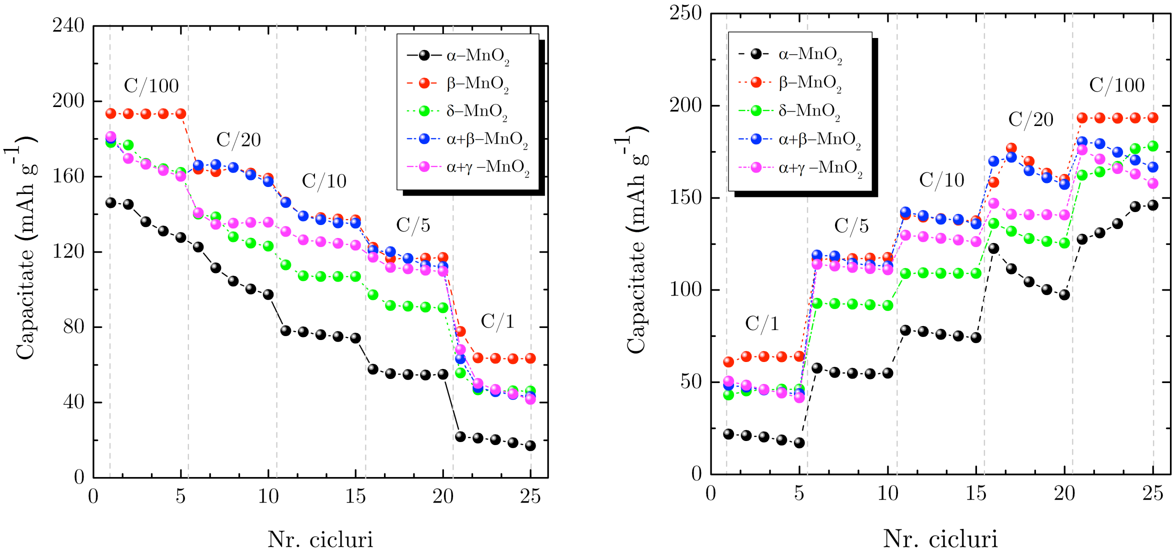

Fig. 8.6 Stability measurements under constant load for different synthetized materials.

Based on galvanostatic measurements β-MnO_2 exhibits intercalation of lithium cations up to the composition $Li_{0.79}[MnO_2]$ resulting a capacity of 239mAh g^{-1} (78% of the theoretical value) at 2.95V at a rate of C/20 and 25°C resulting a power density of 705Wh kg^{-1}. At a discharge rate of C/10 after 100 cycles a drop is observed to a composition of $Li_{0.5}[MnO_2]$ resulting 200Wh kg^{-1}.

Phase pure β-MnO_2 shows best performance in terms of capacity retention and power density among the synthetized materials providing 244mAh g^{-1} at C/100.

8.7 Electrochemical impedance spectroscopy measurements of the ß-MnO2 in $LiPF_6$

Impedance measurements have been undertaken to observe the evolution of internal resistances in correlation with the state of discharge and charge. Capacity loss and irreversibility are generally results of non-electroactive side reactions, phase transformation from an active to an inactive state or by formation of the (SEI) solid electrolyte interface. SEI usually presents lower ion and electronic conductivities witch clearly impact overall battery performance. Nyquist representation of the measured impedances of the system (Fig. 8.8) at different states of charge can be divided in four groups:

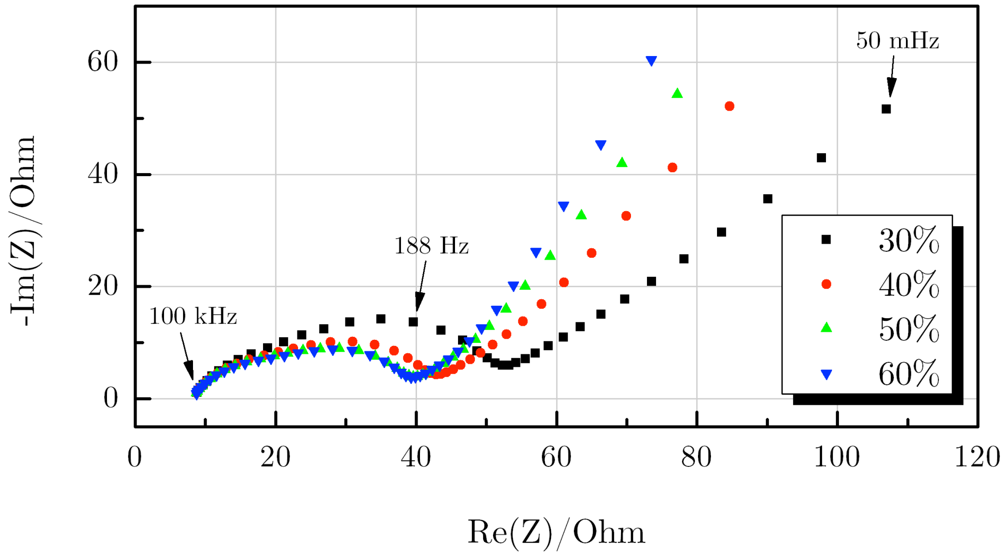

Fig. 8.8 Nyquist diagrams recorded at different state of charge in a Li - β-MnO_2 cell

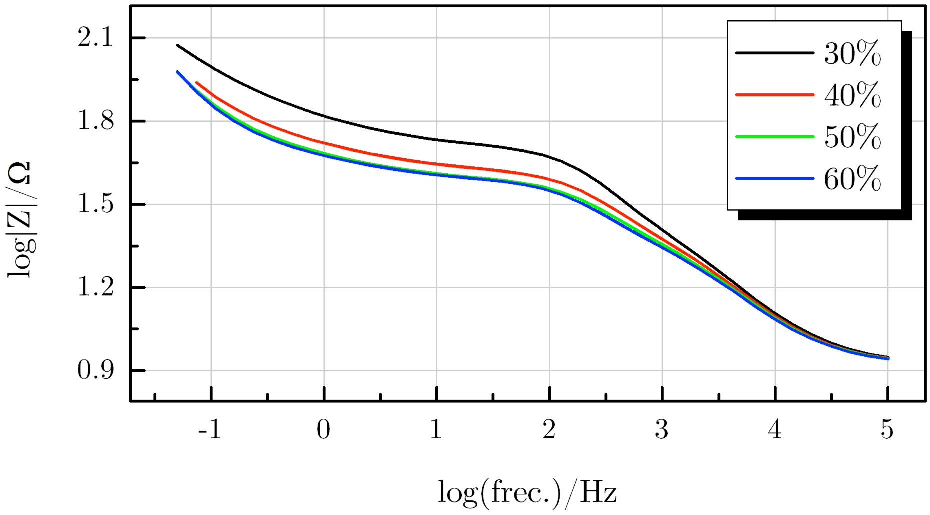

Fig. 8.9 Bode diagram recorded at different state of charge in a Li - β-MnO_2 cell

Nyquist (Fig. 8.8) spectra can be divided as follows:

- The first part is considered the sum of resistances of the current collectors, electroactive material electrolyte and the separator material
- The first semi-circle is attributed to the formation of SIE and it's characteristics
- The second semi-circle is resulted by the charge transfer resistance and capacitive behaviour of the double-layer with some contribution from mass transfer resistance.
- The sloping part is attributed to the Warburg impedance

The equivalent circuit in Fig. 8.10 describes well the phenomena observed during impedance measurements.

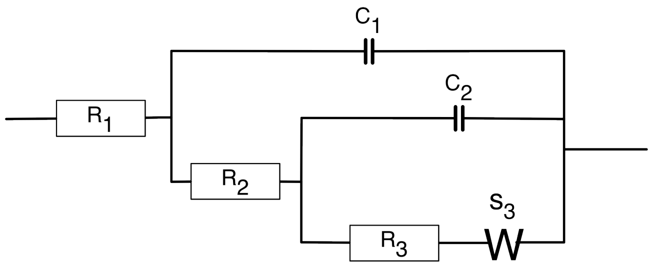

$R_1 = 9.224\ \Omega$
$C_1 = 2.53\ \mu F$
$R_2 = 14.87\ \Omega$
$C_2 = 18.03\ \mu F$
$R_3 = 25.99\ \Omega$
$s_3 = 32.25\ \Omega \bullet s^{\frac{1}{2}}$

Fig. 8.10 Equivalent electric circuitry of the measured cell corresponding to a maximum charge of 30%

9. MATHEMATICAL MODELLING OF THE DISCHARGE OF A Li-MnO_2 CELL

The COMSOL model is based on the model described by (Doyle *et al.*, 1996; Cai and White, 2011) where material balance is given by Fick's second law:

$$\frac{\partial c_{s,i}}{\partial t} = D_{s,i} \frac{1}{r^2} \frac{\partial}{\partial r}\left(r^2 \frac{\partial c_{s,i}}{\partial r} \right) \tag{9.1}$$

Charge balance in the liquid phase is given by Ohm's law:

$$-\frac{\partial}{\partial x}\left(\kappa_{ef,i} \frac{\partial \phi_2}{\partial x} \right) + \frac{2RT(1-t_+^0)}{F} \frac{\partial}{\partial x}\left(\kappa_{ef,i} \frac{\partial \ln c_i}{\partial x} \right) = a_i F J_i \tag{9.19}$$

Material flux in the porous model electrode for spherical particles is controlled by Butler – Volmer kinetic model:

$$J_i = k_i \left(c_{s,i,\max} - c_{s,i,\sup} \right)^{0.5} c_{s,i,\max}^{0.5} c_i^{0.5} \left[\exp\left(\frac{0.5F}{RT} \eta_i \right) - \exp\left(\frac{0.5F}{RT} \eta_i \right) \right] \tag{9.22}$$

9.4 COMSOL model

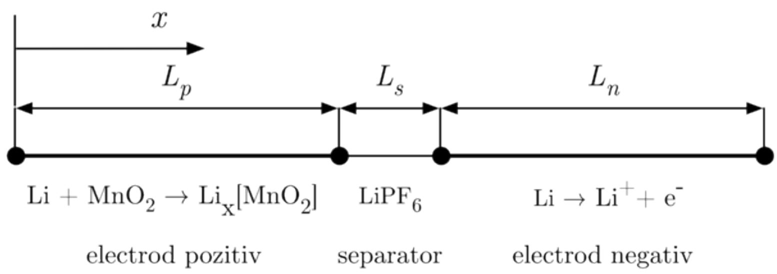

Fig. 9.1 Geometric model of the modelled cell

9.5 Model validation

Refined model has been investigated using experimentally obtained values for a discharge in a Swagelok type cell. As shown in Fig. 9.2 a good overlapping of the simulated data with the experimental can be observed. However, the mathematical model does not well describe effects of the particle sizes in question since experimentally an important contribution of the size reduction has been found. Such behaviour will impact the plateau-like discharge of the material as observed in the experimental data vs. the simulated data.

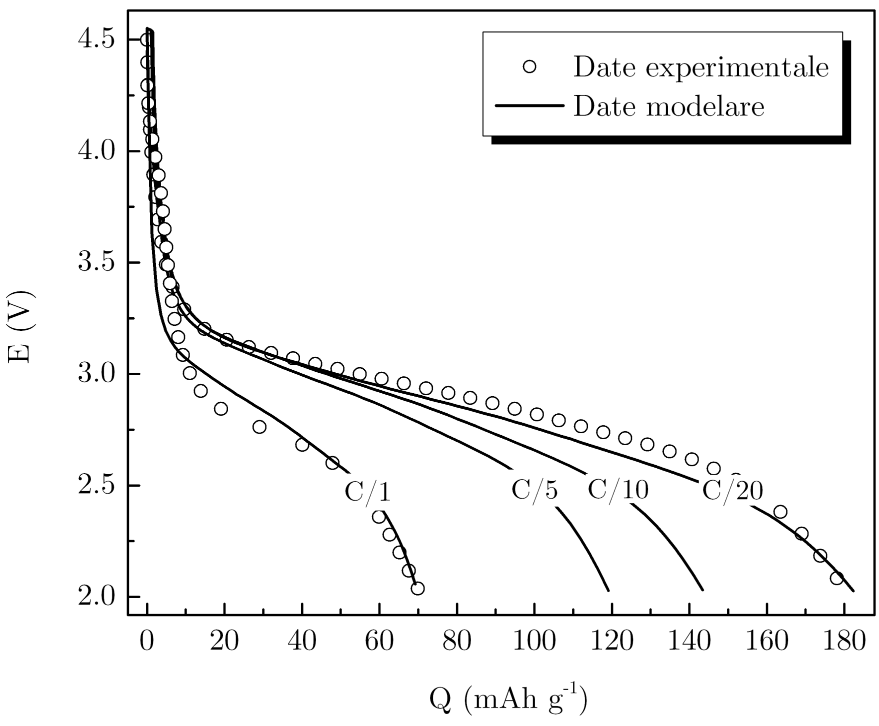

Fig. 9.2 Galvanostatic discharge of a Li-MnO_2 cell at different C rates

10. HYDROMETALLURGICAL PROCESS FLOW FOR SPENT LECLANCHÉ BATTERY RECOVERY

10.3 Unit operations on the spent battery recycling process flux

In the present study, mechanical treatments consist of grinding and sieving followed by magnetic separation, resulting in the reclamation of constructive parts such as: metallic casings (≤99% iron), plastic garments (PVC, HDPE) and cellulose-based separator materials. Metallic zinc is also recovered in this step.

The resulted material is dried in an oven to obtain the needed high fraction of powdered spent battery material for efficient screening as reported by previous researchers (Meador, 1995; Salgado et *al.,* 2003, Vatistas et *al.*, 2001). The grinded constructive parts are subjected to intensive sieving step, where the powdered parts are separated from the rest, leaving the iron casings, metallic zinc anodes, plastics and separators for further processing. Conveying the scraps in a magnetic field successfully separates ferrous parts. Non-ferrous elements are subjected to washing with demineralised water, during which by flotation the cellulose and plastic parts are removed leaving a slightly alkaline aqueous solution with metallic zinc scraps and graphite rods, finally separated by screening.

By crystallization, salts have been also recovered from the washing liquids. By filtration the Zn^{2+} and Mn^{2+} containing liquor is separated from the carbonaceous paste material, leaving a solid phase composed of un-leached manganese oxides and traces of Zn^{2+}

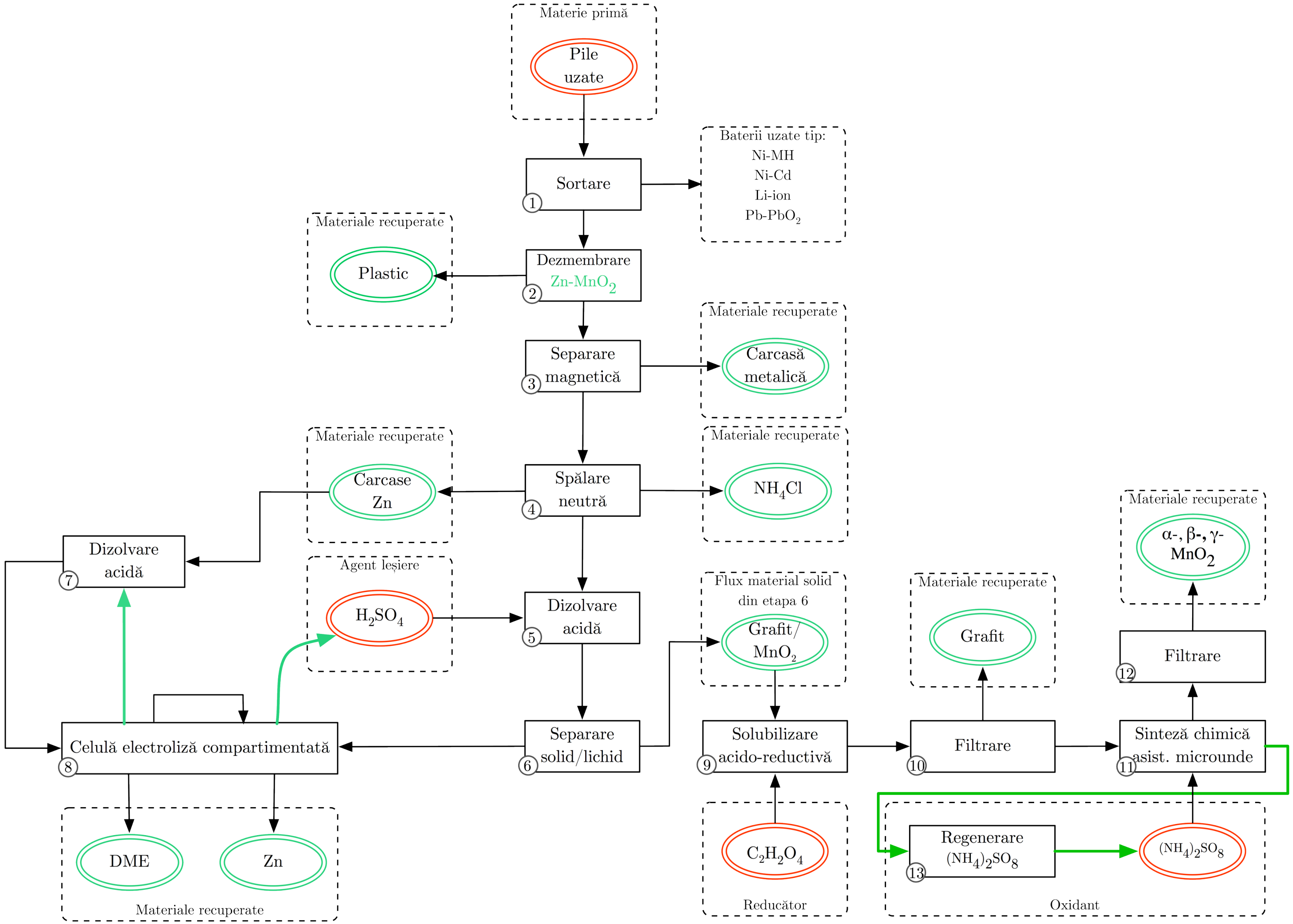

Fig. 10.1 Unit operations in spent Zn – C battery recycling technology by hydrometallurgical treatment route

Unit operation on the spent battery recycling flu are as follows:

1. **Sorting**. Spent batteries are sorted based on their electroactive content Zn-C, Ni-MH, Li-ion, Pb, Ni-Cd, etc.
2. **Disassembly**. Exhausted cells are disassembled in parts such as: (i) plastics; (ii) metallic materials (iii) spent electroactive powder material.
3. **Magnetic** separation. Metallic parts are conveyed in a magnetic field for metallic parts such as protective battery casings recovery.
4. **Neutral washing.** Materials resulted from step 3 are washed in order to extract soluble phases such as NH_4Cl electrolyte to reduce acid consumption in the following operations.
5. **Leaching.** Spent battery powder material is leached with an acidic solution composed of H_2SO_4 1M, in solid-liquid ratio of 1:10, for 60 minute under vigorous stirring in order to extract the metals from the solid to the liquid phase according to the below reactions:

$$ZnO + H_2SO_4 \rightarrow ZnSO_4 + H_2O \tag{10.1}$$

$$Mn_2O_3 + H_2SO_4 \rightarrow MnO_2 + MnSO_4 + H_2O \tag{10.2}$$

6. **Solid liquid separation**.
7. **Leaching.** Unspent Zn casing which are readily available in the feedstock are dissolved in an aqueous solution of 1M H_2SO_4 and represent the catholyte in the electrolysis reactor
8. **Electrolysis** with the following electrode reactions:

$$\text{At the cathode: } Zn^{2+} + 2e^{-} \rightarrow Zn \tag{10.4}$$

With 90% current efficiency and H_2er with 10% current efficiency.

$$\text{At the anode: } MnSO_4 + 2H_2O \rightarrow Mn_3O_4 + H_2SO_4 + 2H^{+} + 2e^{-} \tag{10.5}$$

With 85% current efficiency and O_2er with 15% current efficiency.

9. **Reductive leaching** of the filtrate according to the reaction:

$$MnO_2 + H_2SO_4 + H_2C_2O_4 \rightarrow MnSO_4 + 2H_2O + 2CO_2 \tag{10.6}$$

10. **Filtration** for graphitic material recovery.
11. Microwave assisted hydrothermal synthesis of MnO2 according to the reaction:

$$MnSO_4 + (NH_4)_2S_2O_8 + 2H_2O \rightarrow MnO_2 + (NH_4)_2SO_4 + 2H_2SO_4 \tag{8.2}$$

12. **Filtration** for MnO2 recovery from reaction volume.
13. $(NH_4)_2SO_4$ is regenerated in an electrochemical reactor (Ilea, 2005).

10.4 Mass balances on the process flow

Tab. 10.12 Global mass balance for 100 kg treated spent batteries

Materiale intrate	**kg**	**Materiale ieșite**	**kg**
Metallic parts	12.6	Metallica parts	12.6
Plastic	2.3	Plastic	2.3
Graphite	7.4	Separator	0.6
Separator	0.6	Graphite	7.4
Electrolyte	1.8	Electrolyte	1.8
Metallic Zn	16.5	H_2	0.5
ZnO	10.4	$ZnSO_4$	51.9
MnO_2	15.5	$MnSO_4$	1.0
Mn_2O_3	27.0	H_2O	1068.4
H_2O	1070.7	Mn_3O_4	12.6
H_2SO_4	90.7	O_2	0.2
$C_2H_2O_4$	31.4	H_2SO_4	96.4
$(NH_4)_2S_2O_8$	79.6	Zn	3.8
		CO_2	30.7
		MnO_2	30.4
		$(NH_4)_2SO_4$	46.1
TOTAL	**1366.6**	**TOTAL**	**1366.6**

11. GENERAL CONCLUSIONS

The influence of manganese (II) inclusion was studied on the electrochemical behaviour of commercially pure titanium in acidic electrolytes through open circuit potential measurements. The presence of Mn2+ ions in the acidic electrolyte maintains good
electric conductivity caused by formation of a mixed oxide film on the electrode surface. Based on these assumptions, a titanium surface activation technique was developed which allows MnO2 electrosynthesis. MnO2 deposited during anodic polarization on the titanium surface, act as nucleation centre for the latter developing EMD film. Commercially pure titanium anode surface modification prior to MnO2 electrodeposition from spent battery leach liquors is essential. By surface modification, titanium passivation has been delayed during anodic polarisation, from several tents of minutes as described in the literature, to several hundred minutes in our experimental conditions.

Based on literature information and preliminary experimental results, a hydrometallurgical process flowsheet has been proposed for complete recycling of spent, deteriorated or expired Zn-C batteries. In the studied electrochemical setup high purity nano-metric zinc and Mn_3O_4 has been simultaneously electrodeposited from spent battery leach liquors in an anionic membrane reactor.

By cyclic voltammetry measurements, electrode processes and their impact on the manganese oxide electrowinning from SBLL has been investigated. Electrowinning tests have shown best results in current efficiency terms at a current density of 5A dm^{-2} yielding 91% for zinc and 85% for manganese oxide electrowinning efficiency, consistent with typical plant practice. Obtained values are superior or equal with ones reported (Ault and Frazer, 1988; De Souza, 2004, Zhao and Liu, 2011). Information about structure, composition and morphology of the electro synthetized deposits has been obtained by applying XRD, EDX, SEM and electrochemical measurements revealing phase pure Zn and Mn_3O_4.

Recovery of manganese and zinc from Zn-C batteries through a hydrometallurgical route has been achieved with zero impact on the environment while all electroactive; constructive and chemical parts have been recovered or have been reintroduced in the technological flux.

By leaching reductive leaching of the filtrate resulted from the spent battery leaching liquors, a high Mn^{2+} containing solution has been obtained. These solutions have been tested in the presence of a strong oxidizing agent in a microwave-assisted chemical reactor. Different structural manganese dioxides have been obtained.

Synthetized MnO_2 polymorphs have been tested as intercalation materials in Li-ion cells and exhibit 60 – 70 % of the theoretical values with good rate capabilities and capacity retention for ß-MnO_2 after 100 cycles with a composition of $Li_{0.5}MnO_2$.

The discharge of the Li - MnO_2 has been modelled in COMSOL. The model has approximated experimental data but several phenomenological processes have not been modelled resulting in a less complete overlap.

Based on literature and experimental data a technological flowsheet has been proposed for complete recovery of spent battery components and materials.

From an optimization and environmental point of view both the simultaneous electrochemical electrowinning and the microwave-assisted chemical reactor are of utmost interest. These technologies have been used because of their low energy consumption and ability to yield pure material phases.

References

Agladze, G., Gogishvili, N., Koiava, N., Zaridze, I., 2008. Experimental study of electrolytic metallic manganese and electrolytic manganese dioxide simultaneous electrosynthesis in MA-40 anion exchange membrane reactor. Bull. Georg. Natl. Acad. Sci., 2, 4, 89 – 90.

Adelkhani, H., Ghaemi, M., 2010. Characterization of manganese dioxide electrodeposited by pulse and direct current for electrochemical capacitor, Journal of Alloys and Compounds, 493, 175–178.

Andre, D., Meiler, M., Steiner, K., Wimmer, Ch., Soczka-Guth, T., Sauer, D.U., 2011. Characterization of high-power lithium-ion batteries by electrochemical impedance spectroscopy. I. Experimental investigation, J. Power Sources, 196, 5334–5341.

Anton, M., Manciulea, A.L., Ilea, P., 2011. Comparative study of solubilisation methods for zinc and manganese recovery from spent batteries. Studia Universitatis Babeș-Bolyai Chemia 56, 4, 223 – 233.

Ault, A.R., Frazer, E.J., 1988. Effects of certain impurities on zinc electrowinning in high-purity synthetic solutions. J. Appl. Electrochem., 18, 583 – 589.

Avraamides, J., Senanayake, G., Clegg, R., 2006. Sulfur dioxide leaching of spent zinc-carbon-battery scrap. J. Power Sources, 159, 1488–1493.

Baba, A.A., Adekola, A.F., Bale, R.B., 2009. Development of a combined pyro- and hydro-metallurgical route to treat spent zinc–carbon batteries, J. Haz. Mat., 171, 838–844.

Bai, L., Wang, X., Wang, X., Zhang, X., Long, W., Wang, H., Li, J., 2011. Preparation and Capacitive Behavior of Dandelion-Like γ-MnO2 Nanofibre/Activated Carbon Microbeads Composite for the Application of Supercapacitor. International Journal of Electrochemistry, ID 692603, 1-6.

Bard, A.J., Faulkner, L.R., 2001. Electrochemical Methods Fundamentals and Applications, 2nd edition, John Wiley and Sons.

Bernardes, A.M., Espinosa, D.C.R., Tenório, J.A.S., 2004. Recycling of batteries: a review of current processes and technologies. J. Power Sources 130, 291-298.

Berzelius, J.J., 1817. Ann. Chem. Phys., 6, 204–205.

Bode, H., 1961 Angew. Chem., 73, 553–560.

Bolton, L.G., Sefton, V.B., Zubryckyj, N., 1981. Removal of manganese ions from zinc and manganese containing solutions. United States Patent no. 4290866.

Brüggler, M., 2008. Method for gasification of waste in a rotary hearth furnace and furnace for gasification of waste. European Patent 2003395A2.

Burkin, A.R., Chouzadjian, A.K., 1980. Process for recovering manganese from aqueous acidic sulphate solutions. United States Patent no. 4198377.

Burri. R., Weber, A., 1995. The Wimmis project, J. Power Sources 57, 31-35.

Byström, A.M., 1949. The Crystal Structure of Ramsdellite, an Orthorhombic Modification of MnO_2. Acta Chem. Scand., 3, 163–173.

Cai, L., White, R.E., 2011. Mathematical modeling of a lithium ion battery with thermal effects in COMSOL Inc. Multiphysics (MP) software, J. Power Sources, 196, 5985–5989.

Chen, S., Zhu, J., Wu, X., Han, Q., Wang, X., 2010. Graphene Oxide MnO_2 Nanocomposites for Supercapacitors, ACS Nano, 4, 2822 – 2830.

Chen, W. M., et al., 2012, Controllable synthesis of hollow bipyramid β-MnO_2 and its high electrochemical performance for lithium storage, ACS Appl. Mater. Interfaces, 4, 3047–3053.

Chen, Z., Chen, Y., Zhang, Y., Xu, G., Yang, J., Feng, Y., 2013. Microwave-hydrothermal preparation of a graphene/hierarchy structure MnO_2 composite for a supercapacitor, http://dx.doi.org/10.1016/j.partic.2012.12.008

Cheng, F., Zhao, J., Song, W., Li, C., Ma, H., Chen, J., Shen, P., 2006. Facile Controlled Synthesis of MnO_2 Nanostructures of Novel Shapes and Their Application in Batteries, Inorg. Chem., 45, 2038−2044

Cheret, D., Santen, S., 2007. Battery recycling. United States Patent no. 7169206 B2.

Chabre, Y., Pannetier, J., 1995. Structural and electrochemical properties of proton/MnO2 system, Prog. in Solid State Chem., 23, 1

Demopoulos, G.P., Rosato, L., Wang, Q., 2002. Method for removing manganese from acidic sulfate solutions. United States Patent no. 6391270 B1.

Díaz-Arista, P., Trejo, G., 2006. Electrodeposition and characterization of manganese coatings obtained from an acidic chloride bath containing ammonium thiocyanate as an additive, Surface & Coatings Technology, 201, 16, 3359-3367.

Ding, K., 2010. Preparation of Palladium Particles-decorated Manganese Dioxide and Its Catalysis towards Oxygen Reduction Reaction (ORR), International Journal of Electrochemical Science, 5, 668 – 681.

De Michelis, I., Ferella, F., Karakaya, E., Beolchini, F., Veglio, F., 2007. Recovery of zinc and manganese from alkaline and zinc-carbon spent batteries. J. Power Sources 172, 975–983.

De Souza, C.C.B.M., Tenório, J.A.S., 2004. Simultaneous recovery of zinc and manganese dioxide from household alkaline batteries through hydrometallurgical processing, J. Power. Sources 136, 191–196.

De Wolff, P.M., 1959. Interpretation of some γ-MnO_2 diffraction patterns, Acta Crystallografica, 12, 341.

Devaraj S., Munichandraiah, N., 2008. Effect of Crystallographic Structure of MnO2 on Its Electrochemical Capacitance Properties, J. Phys. Chem. C, 112, 4406-4417.

Dong, X., Wang, X., Wang, J., Song, H., Li, L., Wang, L., Chan-Park, M.B., Li, B. M., Chen, P., 2012. Synthesis of a MnO_2–graphene foam hybrid with controlled MnO2 particle shape and its use as a supercapacitor electrode, Carbon, 50, 13, 4865–4870.

Doyle, M., Gozdz, A.S., Schmutz, C.N., Tarascon, JM., Newman, J., 1996. Comparison of Modeling Predictions with Experimental Data from Plastic Lithium Ion Cells, J. Electrochem. Soc., 6, 1890 – 1903.

Dose, W.M., Lehr, J., Donne, W., 2012. Characterisation of chemically lithiated heat-treated electrolytic manganese dioxide, Mat. Res. Bul., 47, 1827–1834.

Dutra A.J.B., Almeida, I.C.F., 2008. Electrolytic Manganese Dioxide Nucleation and Growth on Titanium Substrates, Materials Science Forum, 570, 114-119

El-Nadi, Y.A., Daoud, J.A., Aly, H.F., 2007. Leaching and separation of zinc from the black paste of spent MnO_2-Zn dry cell batteries. J. Haz. Mat. 143, 2, 328-334.

European Parliament, 2006. Directive 2006/66/EC on waste batteries and accumulators.

Eurostat, 2012. Generation of Batteries and accumulator wastes (WStatR), http:/epp.eurostat.ec.europa.Eu/portal/page/portal/waste/key_waste_streams/batteries

Ferella, F., De Michelis, I., Veglio, F., 2008. Process for the recycling of alkaline and zinc-carbon spent batteries. J. Power Sources 183, 805–811.

Frölich S., Sewing D., 1995. The BATENUS process for recycling mixed battery waste. J. Power Sources 57, 27 – 30.

Furlani, G., Moscardini, E., Pagnanelli, F., Ferella, F., Veglio, F., Toro, L., 2009. Recovery of manganese from zinc alkaline batteries by reductive acid leaching using carbohydrates as reductant, Hydrometallurgy, 99, 115–118.

Gao, H., Xiao, F., Ching, C.B., Duan, H., 2012. High-Performance Asymmetric Supercapacitor Based on Graphene Hydrogel and Nanostructured MnO2 Appl. Mater. Interfaces 2012, 4, 2801−2810.

Gao, J., Lowe, M. A., Abruña, D. H., 2011. Spongelike nanosized Mn_3O_4 as a high-capacity anode material for rechargeable lithium batteries. Chem. Mater. 23, 3223-3227.

Gummow R. J., de Kock, A., Thackeray, M. M., 1994. Improved capacity retention in rechargeable 4 V lithium/lithium-manganese oxide (spinel) cells, Solid State Ionics 69, 59.

Han, R., Xing, S., Ma, Z., Yinsu, W., Gao, Y., 2012. Effect of the $KMnO_4$ concentration on the structure and electrochemical behaviour of MnO_2. J. Mater. Sci. 47, 3822 – 3827.

Hady, Z. A., Pagetti, J., 1976. Anodic behaviour of titanium in concentrated sulphuric acid solutions. Influence of some oxidizing inhibitors, J. Applied Electrochem., 6, 333-338.

Hariprasad, D., Dash, B., Ghosh, M. K., Anand, S., 2009. Mn recovery from medium grade ore using a waste cellulosic reductant. Ind. J. Chemical Technology, 16, 322-327.

Hashem, M., Abdel-Latif, A.M., Abuzeid, H.M., Abbas, H.M., Ehrenberg, H., Farag, R.S., Mauger, A., Julien, C.M., 2011. Improvement of the electrochemical performance of nanosized α-MnO_2 used as cathode material for Li-batteries by Sn-doping, Journal of Alloys and Compounds, 509, 9669–9674.

Hashem, A.M., Abuzeid, H.M., Mikhailova, D., Ehrenberg, H., Mauger, A., Julien, C.M., 2012. Structural and electrochemical properties of alpha-MnO_2 doped with cobalt, Journal of Materials Science, 47, 5, 2479-2485

Hill, L. I., Verbaere, A., Guyomard, D., 2002. Synthesis of α-, β-, and Low Defect γ-Manganese Dioxides Using the Electrochemical-Hydrothermal Method and Study of their Li Insertion Behavior, Journal of New Materials for Electrochemical Systems, 5, 129-133.

Hosseini, S. M. A., Sigh, V. B., 1993. Active-passive behaviour of titanium and titanium alloy (VT-9) in sulphuric acid solutions, Materials Chemistry and Physics, 33, 63-39.

Ilea, P., Popescu, I. C., Urda, M., Oniciu, L., 1997. The electrodeposition of manganese from aqueous solutions of $MnSO_4$. IV: Electrowinning by galvanostatic electrolysis, Hydrometallurgy, 46, 149-156.

Ilea, P., 2005. Electrosinteze anorganice, Casa Cărții de Știință, 167 – 172.

Jia, F., Chen, M., Wang, C., Wang, J., Zheng, J., 2012. Three-dimensional nano MnO2/CB composite and its application for electrochemical capacitor, Materials Letters, 78, 127–130.

Jia, Z., Yuping, D., Hiu, J., Xiaogang, L., Shunhua, L., 2010. The morphology and electromagnetic properties of MnO2 obtained in 8 T high magnetic field, Journal of Crystal Growth, 312, 2788–2794.

Johnson, J. E., Webb, M. S., Thomas, K., Ono, S., Kirschvink, J. L., 2013. Manganese-oxidizing photosynthesis before the rise of cyanobacteria, Proc. of the Nat. Acad. Sci. United States of America, www.pnas.org/cgi/doi/10.1073/pnas.1305530110

Jorgensen, F. R. A., 1970. Cell Voltage during the Electrolytic Production of Manganese Dioxide, J. Electrochem. Soc., 117, 275.

Kelly, E. J., 1982 în: J.O.'M. Bockris, B.E. Conway, R.E. White (Eds.), Modern Aspects of Electrochemistry, Plenum Press, New York, 1982, p. 319.

Khan Y., Durrani, S. K., Mehmood, M., Khan, M. R., 2011. Mild hydrothermal synthesis of γ-MnO nanostructures and their phase transformation to α-MnO nanowires, J. Mater. Res., Vol. 26, No. 17, 2268 - 2275.

Kholmogorov, A. G., Zyzhaev, A. M., Kononov, U.S., Moiseeva, G.A., Pashkov, G.L., 2001. The production of manganese dioxide from manganese ores of some deposits of the Siberian Region of Russia, Hydrometallurgy, 56, 1-11.

Kijima, N., Sakata, Y., Takahasi, Y., Akimoto, J., Kumagi, T., Igarashi, K., Shimizu, T., 2009. Synthesis and lithium ion insertion/extraction properties of hollandite-type MnO_2 prepared by acid digestion of Mn_2O_3, Solid State Ionics, 180, 616 – 620.

Kim, T.H., Senanayake, G., Kang, J.G., Sohn, J.S., Rhee, K.I., Lee, S.W., Shin, S.M., 2009. Reductive acid leaching of spent zinc carbon batteries and oxidative precipitation of Mn-Zn ferrite nanoparticles. Hydrometallurgy, 96, 154–158.

Kleinsorgen, K., Köhler, U., Bouvier, A., Fölzer, A., 1997. Process for the recovery of metals from used nickel/metalhydride storage batteries. United States Patent 5858061.

Kittel, C., 2005. Introduction to Solid State Physics, 8th ed., Wiley-VCH.

Komaba, S., Esasaki, T., Kumagai, N., 2005. Preparation and electrochemical performance of composite oxide of alpha manganese dioxide and Li–Mn–O spinel, Electrochimica Acta, 50, 2297–2305

Kondrashev, Y.D., 1957. Russ. J. Inorg. Chem., 2, 9–18.

Kononov, Y. S., Pashkov, G. L., Patrushev, V. V., Kholmogorov, A. G., Plekhanov, V. P., 2007. Synthesis of electrolytic manganese dioxide on a heated anode, Zhurnal Prikladnoi Khimii, 80, 339 – 340. 13

Kumar, V., Sahu, S. K., Pandey, B. D., 2010. Prospects for solvent extraction processes in the Indian context for the recovery of base metals. A review. Hydrometallurgy 103, 45-53.

Lai, Y., Jiang, L., Li, J., Zhong, S., Lü, X., Peng, H., & Liu, Y., 2010. A novel porous Pb–Ag anode for energy-saving in zinc electro-winning. Hydrometallurgy 102 (1-4), 73–80.

Lain, M.J., 2001. Recycling of lithium ion cells and batteries. J Power Sources 109(1), 736-738.

Landskrona, S., Melin, A.L., Svensson, V.H., 1983. Process for the recovery of metals from the scrap from nickel–cadmium electric storage batteries, US Patent 4401463.

Lee, S. W., Kim, J., Chen, S., Hammond, P. T., Shao-Horn, Y., 2010. Carbon Nanotube /Manganese Oxide Ultrathin Film Electrodes for Electrochemical Capacitors, ACS Nano, 4, 3889 – 3896.

Li, J., Zhao, Y., Wang, N., Ding, Y., Guan, L., 2012. Enhanced performance of a MnO2–graphene sheet cathode for lithium ion batteries using sodium alginate as a binder J . Mater. Chem., 22, 13002 – 13004.

Li W. N., Yuan, J., Shen, X.F., Gomez-Mower, S., Xu, L.-P., Sithambaram, S., Aindow, M., Suib, S.L., 2006. Hydrothermal Synthesis of Structure- and Shape-Controlled Manganese Oxide Octahedral Molecular Sieve Nanomaterials, Adv Funct Mater, 16, 1247-1253.

Li, Z., Liu, N., Yin, L., 2012. Three-dimensional nanohybrids of Mn_3O_4/ordered mesoporous carbons for high performance anode materials for lithium-ion batteries. J. Mater. Chem. 22, 16640-16648.

Li, Y., Wu, J., Zhou, W., Gao, E., 2012. Effects of manganese on routine semen quality parameters: results from a population-based study in China. BMC Public Health, 12, 919

Liu, J.L., Fan, L.Z., Qu, X., 2012. Low temperature hydrothermal synthesis of nano-sized manganese oxide for supercapacitors, Electrochimica Acta, 66, 302–305.

Luo, L., Li, F., Zhu, L., Zhang, Z., Ding, Y., Deng, D., 2012. Non-enzymatic hydrogen peroxide sensor based on MnO2-ordered mesoporous carbon composite modified electrode, Electrochimica Acta, 30, Pages 179–183.

Lütjering, G., Williams, J. C., 2007. Engineering Materials and processes - Titanium – 2nd edition, Springer Verlag.

Ma, C. C., Peres, E. M., 1951. Corrosion resistance of anodized and unanodized titanium, Industrial and Engineering Chemistry, 43, 675–679.

Madison, S. A., Tebo, B. M., Mucci, A., Sundby, B., Luther III, G. W., 2013. Abundant Porewater Mn(III) Is a Major Component of the Sedimentary Redox System, Science, 341, 875 – 878.

Malankar, H., Umare, S.S., Singh, K., Sharma, M., 2010. Chemical composition and discharge characteristics of γ-MnO2 prepared using manganese ore, J Solid State Electrochem, 14, 71 – 82.

Martin, D., Garcia, M.A., Diaz, G., Falgueras, G., 2001. A new zinc solvent extraction application: spent domestic batteries treatment plant. Proceedings of the International Solvent Extraction Conference (ISEC'99), vol. 1, Barcelona, Spain, 201–206.

Masters, I.M., Bolton, G.L., Sefton, V.B., 1979. Electrolytic recovery of zinc and manganese dioxide. Canadian Patent no. 1066656.

McLaughlin, W., Adams, S.T., 1999. Li reclamation process. United States Patent no. 5888463.

Meador, W.R., 1995. The PECOS project. J. Power Sources 57, 37-30.

Metikos M, 1985. Anodic oxidation of titanium: Mechanism of non-stoichiometric oxide formation, Surface Technology, 24, 273 – 283.

Mouri, T., Okada, M., 1993. Novel manganese oxides, production thereof, and use thereof. European Patent no. 0581290 B1.

Nakon, G.D., 2004. Preparation and use of organic extractant for recovery of metal ions from aqueous solutions. United States Patent no. 6692709 B2.

Nayak, P.K., Munichandraiah, N., 2010. Electrochemical insertion of Sr2+ ions onto nano δ-MnO_2 particles, Materials Letters, 64, 1319–1321.

Nguyen, T.T., 1991. Process for the simultaneous recovery of manganese dioxide and zinc, United States Patent 4992149.

Pagnanelli, F., Sambenedetto, C., Furlani, G., Veglio, F., Toro, L., 2007. Preparation and characterisation of chemical manganese dioxide: Effect of the operating conditions, J. Power Sources, 166, 567 - 577.

Pande, A.M., Gupta, K.N., Altekar, V.A., 1982. Single cell extraction of zinc and manganese dioxide from zinc sulphide concentrate and manganese ores, Hydrometallurgy 9, 57–68.

Pasero, D., Reeves, N., West, A. R., 2005. Co-doped Mn_3O_4: a possible anode material for lithium batteries. J. Power Sources 141, 156 – 158.

Pavlov, P.D. and Iordanov, N., 1970. Growth Processes of the Anodic Crystalline Layer on Potentiostatic Oxidation of Lead in Sulfuric Acid, J. Electrochem. Soc., 1103-1109.

Pons, L. and Brenet, J. (1965) Compt. Rend, 260, 2483–2486.

Poranen M. M., Salgado P. S., Koivunen M.R., 2008. Structural explanation for the role of Mn^{2+} in the activity of phi6 RNA-dependent RNA polymerase. Nucleic Acids Res, 20, 6633–6644.

Prime Faraday Technology Watch, 2004. A Review of Power Sources for Mobile Applications, Pera Knowledge, 10 – 23.

Pilla, A. S., Duarte, M.E., Mayer, C. E., 2009. Manganese dioxide electrodeposition in sulphate electrolytes: the influence of ferrous ions, J. Electroanal. Chem., 568, 7 -14.

Rácz, R., Manciulea, A.L., Ilea, P., 2011. Manganese recovery from wastes: I. Manganese and Zinc recovery by electrodeposition from spent battery leach liquors, *"Romanian International Conference on Chemistry and Chemical Engineering", RICCCEXVII,* Sinaia, România.

Rácz, R., Manciulea, A.L., Ilea, P., 2011. Electrochemical behaviour of metallic titanium in MnO_2 electrosynthesis from synthetic solutions simulating spent battery leach liquors. Studia Universitatis Babeș-Bolyai Chemia, 56, 211 – 222.

Rácz, R., Ilea, P., 2013a. Electrolytic recovery of Mn_3O_4 and Zn from sulphuric acid leach liquors of spent zinc–carbon–MnO_2 battery powder, Hydrometallurgy, 139, 116 – 123.

Rácz, R., Glass, I., Jähne, C., Ilea, P., Klingeler, R., 2013b. Microwave synthesis of MnO_2 polymorphs as high performance intercalation materials in Li|Li^+ electrochemistry, *manuscris*

Raghavan, R., Upadhyay, R.N., 1999. Innovative hydrometallurgical processing technique for industrial zinc and manganese process residues, Hydrometallurgy, 51, 207 – 226.

Recéndiza, A., Navaa, J. L., Gonzáleza, I., 2008. Electrochemical Characterization of MnO_2 Anodically Formed During the Zinc Electrowinning Process, ECS Transactions, 15, 79-89

Reddy, R.N., Reddy, R.G., Sol–gel MnO_2 as an electrode material for electrochemical capacitors, 2003. J. Power Sources, 124, 330–337.

Ren, Ya, 2011. Graphene/δ-MnO2 composite as adsorbent for the removal of nickel ions from wastewater, Chemical Engineering Journal 175, 1 – 7.

Rickelton, W.A., Boyle, R.J., 1990. The selective recovery of zinc with new thio-phosphinic acids. Solvent Extraction and Ion Exchange, 8, 6, 783–797.

Rodrigues, S., Munichandraiah, N., Shukla, A. K., 1998. A cyclic voltammetric study of the kinetics and mechanism of electrodeposition of manganese dioxide, Journal of Applied Electrochemistry, 28, 1235 – 1241.

Salgado, A.L., Veloso, A.M.O., Pereira, D.D., Gontijo, G.S., Salum, A., Mansur, M.B., 2003. Recovery of zinc and manganese from spent alkaline batteries by liquid–liquid extraction with Cyanex 272. J. Power Sources 115, 367–373.

Sayilgan, E., Kukrer, T., Ferella, F., Akcil, A., Veglio, F., Kitis, M., 2009. Reductive leaching of manganese and zinc from spent alkaline and zinc-carbon batteries in acid media. Hydrometallurgy, 97, 73–79.

Sayilgan, E., Kukrer, T., Civelekoglu, G., Ferella, F., Akcil, A., Veglio, F., Kitis, M., 2009. A review of technologies for the recovery of metals from spent alkaline and zinc–carbon batteries, Hydrometallurgy, 97, 158–166.

Sayilgan, E., Kukrer, T., Yigit, N.O., Civelekoglu, G., Kitis, M., 2010. Acid leaching and precipitation of zinc and manganese from spent battery powders using various reductants. J. Hazardous Materials, 173, 137 – 143.

Schlörb, H., Bungs, M., Plieth, W., 1997 H. Schlörb, M. Bungs, and W. Plieth, Synthesis and electrochemical studies of manganese oxides with spinel structure in aqueous electrolyte (9 M KOH), Electrochimica Acta, 42, 2619 – 2625.

Senanayake, G., Shin, S.M., Senaputra, A., Winn, A., Pugaev, D., Avraamides, A., Sohn, J-S., Kim, D-J., 2010. Comparative leaching of spent zinc-manganese-carbon batteries using sulfur dioxide in ammoniacal and sulfuric acid solutions. Hydrometallurgy, 105, 1, 36-41.

Serstevens, A., 2001. Method for recycling and treating of salt and alkaline batteries. European Patent no. 1148571.

Shin, S.M., Senanayake, G., Sohn, J.S., Kang, J.G., Yang, D.H., Kim, T.H., 2009. Separation of zinc from spent zinc-carbon batteries by selective leaching with sodium hydroxide. Hydrometallurgy, 96, 349–353.

Skopov, S. V., Naboichenko, S. S., Galkova, L. I., 2009. The effect of quality of anodes on the process of electrolytic of manganese dioxide, Tsvetnaya Metallurgiya, 1, 25-27. 15

Sloop, S.E., 2010. System and method for removing an electrolyte from an energy storage and/or conversion device using a supercritical fluid. United States Patent no. 7858216

Steffens, H. D., Brune, M., Vacuum-Plasma-Sprayed Titanium-Manganese Electrode Layersfor MnO_2 Deposition, Journal of Thermal Spray Technology, 4, 85 – 88.

Stern, M., Geary, A. L., 1957. Electrochemical Polarization I. A Theoretical Analysis of the Shape of Polarization Curves. Journal of Electrochemical Society, 104, 56 - 57.

Sumboja, A., Tefashe, U.M., Wittstock, G., Lee, P.S., 2012. Monitoring electroactive ions at manganese dioxide pseudocapacitive electrode with scanning electrochemical microscope for supercapacitor electrodes", J. Power Sources 207, 205-211.

Tanii, T., Tsuzuki, S., Honmura, S., Kamimura, T., Sasaki, K., Yabuki, M., Nishida, K., 2003. Method for crushing cell.United States Patent no. 6524737.

Tedjar, F., Foudraz J.C., 2007. Method for the mixed recycling of lithium-based anode batteries and cells. United States Patent no. 7820317.

Thackery, M.M., 1997. Manganese oxides for lithium batteries, Progress in Solid State Chemistry, 25, 1-71.

Thackery, M.M., David, W.I.F., Bruce, P.G., Goodenough, J.B., 1983. Lithium insertion into manganese spinels. J. B. Mater. Res. Bull., 18, 461 - 472.

Toro, L., Veglio, F., Beolchini, F., Zanetti, M., Furlani, G., 2006. Process and plant for the treatment of run-down batteries. European Patent no. 1684369A1.

USEPA, 2012. http://www.epa.gov/wastes/conserve/materials/battery.htm.

USEPA, Iris, 0373, 2013. http://www.epa.gov/iris/subst/0373.htm.

Utomo, W.B., Donne, S.W., 2006. Electrochemical behaviour of titanium in H_2SO_4 – $MnSO_4$ electrolytes, Electrochimica Acta, 51, 3338-3345. 16

Van Erkel, J., 2002. Recovery of cadmium and nickel from batteries. United States Patent no. 5407463.

Vatistas, N., Bartolozzi, M., Arras, S., 2001. The dismantling of spent alkaline zinc manganese dioxide batteries and the recovery of the zinc from the anodic material. J. Power Sources, 101, 182 – 187

Veglio, F., Trifoni, M., Aburuzzese, C., Toro, L., 2001. Column leaching of a manganese dioxide ore: a study by using fractional factorial design. Hydrometallurgy, 59, 31-44.

Veloso, L.R.S., Rodrigues, L.E.O.C., Ferreira, D.A., Magalhaes, F.S., Mansur, M.B., 2005. Development of a hydrometallurgical route for the recovery of zinc and manganese from spent alkaline batteries. J. Power Sources 152, 295-302.

Verbaan, B., Mullinder, B., 1981. The simultaneous electrowinning of manganese dioxide and zinc from purified neutral zinc sulphate at high current efficiencies. Hydrometallurgy, 7, 339-352.

Victor, V. De, Pomerantseva, E., Kulova, T.L., Grigorieva, A.V., Skundin, A.M., Goodilin, E.A., Tretyakov, Y.D., 2009. Synthesis, chemical modification and electrochemical behaviour of layered sodium manganese dioxide, Mendeleev Commun., 19, 187 – 189.

Wang, C., Yin, L., Xiang, D., Qi, Y., 2012. Uniform carbon layer coated Mn_3O_4nanorod anodes with improved reversible capacity and cyclic stability for lithium ion batteries. ACS Appl. Mater. Interfaces, 4, 1636 – 1642.

Wang, H., Cui, L.F., Yang, Y.A., Casalongue, H.S., Robinson, J.T., Liang, Y.Y., Cui, Y., Dai, H.J., 2010. Mn_3O_4-Graphene Hybrid as a High-Capacity Anode Material for Lithium Ion Batteries. J. Am. Chem. Soc., 132, 13978 – 13980.

Wang, N., Cao, X., Lin, G., Shihe, Y., 2007. λ-MnO2 nanodisks and their magnetic properties Nanotechnology, 18, 475605.

Wang, Y., Liu, H., Sun, X., Zhitomirsky, I., 2009. Manganese dioxide–carbon nanotube nanocomposites for electrodes of electrochemical supercapacitors, Scripta Materialia, 61, 1079–1082.

Wang, Y., Yu, S.F., Sun, C.Y., Zhu, J.T., Yang, Y.H., 2012. MnO_2/onion-like carbon nanocomposites for pseudocapacitors, J. Materials Chemistry, 22, 17584.

Wark, I.W., 1963. Influence of cobalt on the electrodeposition of zinc. Proceedings of the First Australian Conference on Electrochemistry, Pergamon, 889 - 900.

Wei, Q., Ren, X., Du, J., Wei, S., Hu, S., 2010. Study of the electrodeposition conditions of metallic manganese in an electrolytic membrane reactor, Minerals Engineering, 23, 578–586.

Welz, B., Sperling, M., Resano, M., 1998. Atomic absorption Spectrometry, 3rd ed., Wiley-VCH

WHO, *IARC* Monographs, 2013. http://monographs.iarc.fr/ENG/Classification/index. php.

Williams, M., Todd, G. D., Roney, N., et al., 2012. Toxicological Profile for Manganese, Atlanta (GA): Agency for Toxic Substances and Disease Registry (US); http://www.ncbi.nlm.nih.gov/books/NBK158871/

Zenger, T., Krebs, A., van Deutekom, H.J.H., 2010. Method of and apparatus for dismantling and storage of objects comprising alkali metals, such as alkali metal containing batteries. United States Patent no. 7833646 B2.

Zhang, W., Ren, X., Yang, Z., Wang, Q., Huang, F., 2007. Hydrothermal synthesis of crystalline α-/β-MnO2 nanorods via γ-MnOOH nanorod precursors, Front. Chem. Eng. China, 1, 365–371.

Zhang, W., Cheng, C.Y., 2006. Manganese metallurgy, recovery and control — a literature review. Part I: Manganese Metallurgy, CSIRO Minerals, Australia, DMR - 2809

Zhang, W., Cheng, C.Y., 2007. Manganese metallurgy review. Part I: Leaching of ores/secondary materials and recovery of electrolytic/chemical manganese dioxide, Hydrometallurgy, 89, 137–159.

Zhang, W., Cheng, C.Y., 2007. Manganese metallurgy review. Part II: Manganese separation and recovery from solution, Hydrometallurgy 89, 137–159.

Zhang, W., Cheng, C.Y., 2007. Manganese metallurgy review. Part III: Manganese control in zinc and copper electrolytes, Hydrometallurgy 89, 137–159.

Zhang, Q. B., Hua, Y., 2009. Effect of Mn^{2+} ions on the electrodeposition of zinc from acidic sulphate solutions, Hydrometallurgy, 99, 249 – 254.

Zhang, Q.H., Sun, S., Li, S., Jiang, H., Yu, J.G., 2007. Adsorption of lithium ions on novel nanocrystal MnO_2, Chemical Engineering Science, 62, 4869–4874.

Zhang, X., Sun, X., Zhang, H., Zhang, D., ma, Y., 2013. Microwave-assisted reflux rapid synthesis of MnO_2 nanostructures and their application in supercapacitor, Electrochimica Acta, 87, 637-644.

Zhao, G., Liu, Q., 2011. Effects of impurities ions on zinc electrowinning process in alkaline leaching. IPCBEE vol. 1, IACSIT Press, 397 – 400.

Zhou, M., Zhang, X., Wei, J., Zhao, S., Wang, L., Feng, B., 2011. Morphology controlled synthesis and novel microwave absorption properties of hollow urchinlike alpha-MnO_2 nanostructures, J. Physical Chemistry C, 115, 1389 – 1402.

Zhu, J., Shi, W., Xiao, N., Rui, X., Tan, H., Lu, X., Hng, H.H., Ma, J., Yan, Q., 2012. Oxidation-Etching Preparation of MnO2 Tubular Nanostructures for High-Performance Supercapacitors, Appl. Mater. Interfaces, 4, 2769—2774.

Xia, H., Wang, Y., Lin, J., Lu, L., 2012. Hydrothermal synthesis of MnO_2/CNT nanocomposite with a CNT core/porous MnO_2 sheath hierarchy architecture for supercapacitors, Nanoscale Research Letters, 9, 7 – 33.

Xiao, L., Yang, Y., Yin, J., Li, Q., Zhang, L., 2009. Low temperature synthesis of flower-like $ZnMn_2O_4$ superstructures with enhanced electrochemical lithium storage. J. Power Sources, 194, 1089 – 1093.

Yamaji, N., Sasaki, A., X, J. X., Yokosho, K., Ma, J. F., 2013. A node-based switch for preferential distribution of manganese in rice, Nature Communications, 4, doi: 10.1038/ncomms3442

Ye, K.H., Z.Q., Xu, C.W., Li, N., Chen, Y.B., Su, Y.Z., 2013. MnO_2/reduced graphene oxide composite as high-performance electrode for flexible supercapacitors, Inorganic Chemistry Communications, 30, 1–4.

Yousefi, T., Golikand, A.N., Hossein Mashhadizadeh, M., Aghazadeh, M., 2012. Facile synthesis of α-MnO_2 one-dimensional (1D) nanostructure and energy storage ability studies, Journal of Solid State Chemistry, 190, 202-207.

Yi, L., Zhang, J., Qian, Y., 2006. A simple method of fabricating large-area α-MnO2 nanowires and nanorods, Journal of Solid State Chemistry, 179, 1757–1761.

Yu, P., O'Keefe, T.J., 2002. Evaluation of lead anode reactions in acid sulphate electrolytes II. Manganese reactions, J. Electrochem.Soc., 149, 558 – 569.

Yuping, D., He, M., Xiaogang, L., Shunhua, L., Zhijlang, J., 2010. The microwave electromagnetic characteristics of manganese dioxide with different crystallographic structures, Physica B - Condensed Matter, 405, 1826–1831.